

1 Identification of highly oxygenated organic molecules and their role in 2 aerosol formation in the reaction of limonene with nitrate radical

3 Yindong Guo¹, Hongru Shen¹, Iida Pullinen^{2, a}, Hao Luo^{1,3}, Sungah Kang², Luc Vereecken², Hendrik Fuchs², Mattias
4 Hallquist⁴, Ismail-Hakki Acir^{2, b}, Ralf Tillmann², Franz Rohrer², Jürgen Wildt², Astrid Kiendler-Scharr², Andreas
5 Wahner², Defeng Zhao^{1,5,6*}, Thomas F. Mentel^{2*}

6 ¹Department of Atmospheric and Oceanic Sciences & Institute of Atmospheric Sciences, Fudan University, 200438,
7 Shanghai, China

8 ²Institute of Energy and Climate Research, IEK-8: Troposphere, Forschungszentrum Jülich GmbH, 52425, Jülich,
9 Germany

10 ³IRDR ICoE on Risk Interconnectivity and Governance on Weather/Climate Extremes Impact and Public Health,
11 Fudan University, Shanghai 200438, China

12 ⁴Department of Chemistry and Molecular biology, University of Gothenburg, Göteborg, 41258, Sweden

13 ⁵Shanghai Frontiers Science Center of Atmosphere-Ocean Interaction, Fudan University, Shanghai 200438, China

14 ⁶Institute of Eco-Chongming (IEC), 20 Cuiniao Rd., Chongming, Shanghai, 202162, China

15 ^a Now at: Department of Applied Physics, University of Eastern Finland, Kuopio, 70210, Finland.

16 ^b Now at: Institute of Nutrition and Food Sciences, University of Bonn, Bonn, 53115, Germany.

17 *Correspondence to:* Defeng Zhao (dfzhao@fudan.edu.cn), Thomas F. Mentel (t.mentel@fz-juelich.de)

18
19 **Abstract.** Nighttime NO₃-initiated oxidation of biogenic volatile organic compounds (BVOC) such as monoterpenes
20 is important for the atmospheric formation and growth of secondary organic aerosol (SOA), which has significant
21 impact on climate, air quality and human health. In such SOA formation and growth, highly oxygenated organic
22 molecules (HOM) may be crucial, but their formation pathways and role in aerosol formation have yet to be clarified.
23 Among monoterpenes, limonene is of particular interest for its high emission globally and high SOA yield. In this
24 work, HOM formation in the reaction of limonene with nitrate radical (NO₃) was investigated in the SAPHIR
25 chamber (Simulation of Atmospheric PHotochemistry In a large Reaction chamber). About 280 HOM products were
26 identified, grouped into 19 monomer families, 11 dimer families and 3 trimer families. Both closed-shell products
27 and open-shell peroxy radicals (RO₂•) were observed, and many of them have not been reported previously.
28 Monomers and dimers accounted for 47 % and 47 % of HOM concentrations, respectively, with trimers making up
29 the remaining 6%. In the most abundant monomer families, C₁₀H₁₅₋₁₇NO₆₋₁₄, carbonyl products outnumbered
30 hydroxyl products, indicating the importance of RO₂• termination by unimolecular dissociation. Both RO₂•
31 autoxidation and alkoxy-peroxy pathways were found to be important processes leading to HOM. Time-dependent
32 concentration profiles of monomer products containing nitrogen showed mainly second-generation formation
33 patterns. Dimers were likely formed via the accretion reaction of two monomer RO₂•, and HOM-trimers via the
34 accretion reaction between monomer RO₂• and dimer RO₂•. Trimers are suggested to play an important role in new

35 particle formation (NPF) observed in our experiment. A HOM yield of $1.5\%_{-0.7}^{+1.7}\%$ was estimated considering only
36 first-generation products. SOA mass growth could be reasonably explained by HOM condensation on particles
37 assuming irreversible uptake of ultra-low volatility organic compounds (ULVOC), extremely low volatility organic
38 compounds (ELVOC) and low volatility organic compounds (LVOC). This work provides evidence for the important
39 role of HOM formed via the limonene + NO₃ reaction in NPF and growth of SOA particles.

40

41 **1 Introduction**

42 The nitrate radical (NO₃) is an important nighttime oxidant in tropospheric chemistry, and can reach mixing ratios of
43 several hundred pptv during nighttime (Seinfeld and Pandis, 2006). It can react with volatile organic compounds
44 (VOC) and is especially reactive to alkenes, where the nitrate radical can undergo an addition reaction to the C=C
45 double bond (Finlayson-Pitts and Pitts, 1997; Seinfeld and Pandis, 2006). Biogenic monoterpenes (C₁₀H₁₆) are a large
46 contribution to the alkenes in the atmosphere (Klinger et al., 2002; Guenther et al., 2012), and their major nighttime
47 loss pathway is reaction with NO₃ (Beaver et al., 2012; Rollins et al., 2012; Ayres et al., 2015; Fry et al., 2013). The
48 chemistry of monoterpenes with NO₃ has implications on the cycle of reactive nitrogen and thus on ozone formation
49 (Brown and Stutz, 2012). Furthermore, since the NO₃ radical is formed through the reaction of NO₂ with O₃, it is
50 considered to be of anthropogenic origin, and reactions of NO₃ with biogenic VOC (BVOC) thus represent an
51 important interaction between biogenic emissions and anthropogenic emissions.

52 The reaction of NO₃ with monoterpenes can form secondary organic aerosols (SOA), which can have a large
53 impact on global climate, air quality and human health (Hallquist et al., 2009; Shrivastava et al., 2017). Laboratory
54 studies showed that monoterpenes have high SOA yields in the reaction with NO₃ due to the low volatility of
55 oxidation products (Ng et al., 2008; Rollins et al., 2009; Fry et al., 2013; Fry et al., 2014; Ayres et al., 2015; Jokinen
56 et al., 2015; Zhou et al., 2015; Boyd et al., 2015; Nah et al., 2016; Boyd et al., 2017; Slade et al., 2017; Clafin and
57 Ziemann, 2018; Bates et al., 2022; Dam et al., 2022). Field studies also showed that nighttime NO₃-initiated oxidation
58 of monoterpenes contributes significantly to SOA in forested regions influenced by anthropogenic emissions (Pye et
59 al., 2010; Rollins et al., 2012; Fry et al., 2013; Ayres et al., 2015; Zhou et al., 2015; Xu et al., 2015; Lee et al., 2016;
60 Zhang et al., 2018; Chen et al., 2020) and potentially in urban areas due to the extensive usage of so-called volatile
61 chemical products (VCP) (Nazaroff and Weschler, 2004; McDonald et al., 2018). For example, the Southern Oxidant
62 and Aerosol Study (SOAS) showed that the BVOC + NO₃ reactions were a substantial source of SOA (Ayres et al.,
63 2015; Xu et al., 2015; Lee et al., 2016; Massoli et al., 2018). Therefore, accurate predictions and evaluations of SOA
64 concentration and thus its climate and environmental effects require a comprehensive understanding of the reactions
65 of monoterpenes with NO₃.

66 Recently, a class of organic compounds named highly oxygenated molecules (HOM) have been shown to be
67 critical substances in the SOA formation from BVOC oxidation, particularly monoterpenes, featuring high O/C ratio
68 and low to extremely low volatility (Ehn et al., 2014; Tröstl et al., 2016; Kirkby et al., 2016; Bianchi et al., 2019).
69 HOM here refers to compounds formed in the gas phase via autoxidation which contain at least six oxygen atoms

70 (Bianchi et al., 2019). Most HOM are classified as ULVOC/ELVOC or LVOC (Bianchi et al., 2019) according to the
71 classification of atmospheric organics based on their volatility (saturation concentration, C^*) by Donahue et al. (2012)
72 (extremely low volatility organic compounds (ELVOC), low volatility organic compounds (LVOC), semi-volatile
73 organic compounds (SVOC), intermediate volatility organic compounds (IVOC), volatile organic compounds
74 (VOC)), and a recent update by Schervish and Donahue (2020) (ultra-low volatility organic compounds (ULVOC)).
75 And thus, HOM can be a substantial contribution to growth of SOA particles through gas-particle partitioning.

76 A better description of the HOM formation chemistry in the oxidation of monoterpenes by NO_3 will improve
77 our understanding of the role of HOM in SOA formation, as well as the relationship between oxidation products,
78 SOA formation and reaction systems. Field observation campaigns as well as laboratory experiments have proven
79 the important contribution of HOM in monoterpene + NO_3 SOA (Lee et al., 2016; Faxon et al., 2018). In the SOAS
80 campaign, HOM-ON (organic nitrates) were identified in both gas and particle phase using a NO_3^- -Chemical
81 Ionization time-of-flight Mass Spectrometer (CI-API-TOF) and a High Resolution Time-of-Flight Chemical
82 Ionization Mass Spectrometer (HR-ToF-CIMS) coupled to a Filter Inlet for Gases and AEROSols (FIGAERO).
83 Species with the sum formula $\text{C}_{10}\text{H}_{15,17,19}\text{NO}_{4-11}$ were observed which are formed through the oxidation of
84 monoterpenes by NO_3 (Lee et al., 2016; Massoli et al., 2018). In a campaign in a boreal forest in Hyytiälä,
85 measurement using a NO_3^- -CI-API-TOF and positive matrix factor (PMF) analysis showed a nighttime factor of
86 HOM-ON formed via NO_3 oxidation of monoterpenes (Yan et al., 2016). Besides the observations at forested regions,
87 monoterpene-derived HOM via NO_3 oxidation also contribute to organic aerosols in urban regions. For example, Liu
88 et al. (2021) and Nie et al. (2022) have found that HOM derived from monoterpene nighttime chemistry are important
89 in megacities in China, especially during summertime. A number of laboratory studies have reported HOM formation
90 by the oxidation of monoterpenes with NO_3 . Boyd et al. (2015) observed $\text{C}_{10}\text{H}_{17}\text{NO}_{4/5}$ and $\text{C}_{10}\text{H}_{15}\text{NO}_{5/6}$ in the gas
91 phase in β -pinene + NO_3 experiments using a quadrupole chemical ionization mass spectrometer with I^- as the reagent
92 ion (I^- -CIMS). They proposed possible formation schemes of these ONs. Nah et al. (2016) further detected 5 and 41
93 HOM-ON in the NO_3 oxidation of α -pinene and β -pinene, respectively, such as $\text{C}_{10}\text{H}_{15/17/19}\text{NO}_{4-9}$ in the gas- and
94 particle-phase using I^- -FIGAERO HR-ToF-CIMS. Clafin and Ziemann (2018) provided formation mechanisms for
95 HOM-ON via gas-phase and particle-phase reactions in the β -pinene + NO_3 reaction system, where particle-phase
96 products were analyzed using reversed-phase high-performance liquid chromatography equipped with a UV-vis
97 photodiode array detector (HPLC-UV), Electron-Ionization Thermal Desorption Particle Beam Mass Spectrometer
98 (EI-TDPBMS), Chemical Ionization Finnigan PolarisQ Ion Trap Mass Spectrometer (CI-ITMS), and Electrospray-
99 Ionization Mass Spectrometer (ESI-MS). Recently, Shen et al. (2021) found a large number of HOM (>150 species)
100 in the β -pinene + NO_3 reaction using NO_3^- -CI-API-TOF. HOM formed in the reaction of four monoterpenes (α -
101 pinene, β -pinene, Δ -3-carene, and α -thujene) with NO_3 were also detected using NO_3^- -CI-API-TOF by Dam et al.
102 (2022). Bell et al. (2021) found that dimer dinitrates ($\text{C}_{20}\text{H}_{32}\text{N}_2\text{O}_{8-13}$) contribute a large portion to SOA from α -pinene
103 + NO_3 and also detected monomer ON such as $\text{C}_{10}\text{H}_{15}\text{NO}_{5-10}$ and $\text{C}_{10}\text{H}_{14,16}\text{N}_2\text{O}_{7-11}$) using FIGAERO-CIMS and an
104 Extractive ElectroSpray Ionization time-of-flight mass spectrometer (EESI-ToF-MS). The detailed speciation

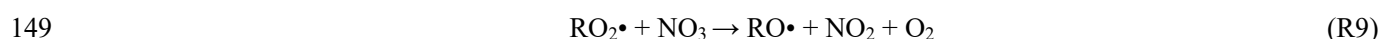
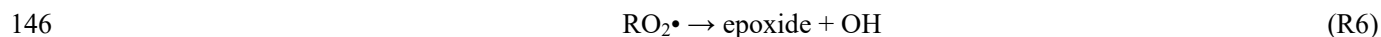
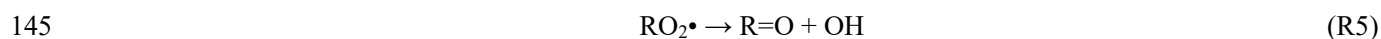
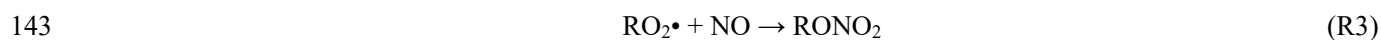
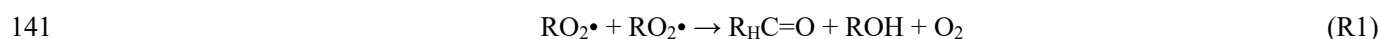
105 depends on analytical method to some extent, though. Moreover, the HOM composition in the particle-phase was
106 found to depend on aging time and reaction conditions such as dark versus light (Bell et al., 2021; Wu et al., 2021a).

107 Among the monoterpenes, understanding the reaction system of limonene with NO₃ is of specific importance.
108 The emission of limonene makes the 4th largest contribution with an estimated global emission of 11.4 Tg annually,
109 preceded only by α -pinene, trans- β -ocimene and β -pinene (Guenther et al., 2012). Besides its biogenic origin,
110 limonene is also a common additive in cleaning products (Nazaroff and Weschler, 2004) and can even be used as a
111 tracer for fragrances in some places (Gkatzelis et al., 2021). Several studies have shown adverse health effects due
112 to indoor pollution caused by the ozonolysis of limonene (Clausen et al., 2001; Fan et al., 2003; Carslaw et al., 2012;
113 Pagonis et al., 2019). Moreover, limonene stands out with its high reactivity towards the NO₃ radical (with a lifetime
114 of 3 min at 298 K at 20 pptv NO₃) (Ziemann and Atkinson, 2012), and NO₃ oxidation of limonene has high SOA
115 yield (SOA mass yield 15 to 231 %) (Hallquist et al., 1999; Spittler et al., 2006; Fry et al., 2011; Fry et al., 2014;
116 Boyd et al., 2017; Berkemeier et al., 2020; Mutzel et al., 2021). A number of earlier studies have provided valuable
117 insights into the reaction of limonene with NO₃ regarding its main products and their formation pathways, the SOA
118 yield, and the SOA physicochemical properties. For example, Hallquist et al. (1999) measured the SOA mass yield
119 and revealed the dominance of organic nitrates (ON) and carbonyl compounds in the products. Fry et al. (2011)
120 determined the organic nitrate yield and proposed a reaction scheme leading to the formation of ON and carbonyls,
121 and Fry et al. (2014) compared the SOA and ON yields from the NO₃ oxidation of α -pinene, β -pinene, and limonene,
122 and demonstrated why limonene + NO₃ leads to more SOA and ON than α -pinene from a structural perspective. Boyd
123 et al. (2017) found a higher N:C ratio for limonene + NO₃ SOA than for β -pinene + NO₃ SOA. Finally, Peng et al.
124 (2018) studied the optical properties of the limonene + NO₃ SOA.

125 Regarding the HOM formation in the reaction of limonene with NO₃, Faxon et al. (2018) reported a series of
126 HOM in the particle phase, including C₇₋₁₀ monomers with 3-11 oxygen atoms and C₁₁₋₂₀ dimers with 5-19 oxygen
127 atoms using I-FIGAERO HR-ToF-CIMS. However, identification of gas-phase HOM products in the limonene +
128 NO₃ reaction is still lacking and their formation mechanisms remain unclear. Theoretical investigations have revealed
129 that NO₃ addition on the endocyclic C=C double bond is more favorable than the exocyclic one due to a lower energy
130 barrier (Jiang et al., 2009), and this endocyclic double bond of limonene thus tends to be attacked by NO₃ and leads
131 to products including hydroxy-substituted ON or diketone products. The remaining exocyclic double bond can also
132 be attacked by NO₃ in secondary chemistry, leading to more functionalized products (Fry et al., 2011).

133 The formation of HOM via autoxidation involves a sequence of multiple intramolecular H-shift and O₂ addition
134 reactions, and results in highly oxygenated peroxy radicals (HOM-RO₂•) (Ehn et al., 2014). These HOM-RO₂• can
135 react similarly to traditional RO₂• (Bianchi et al., 2019). The bimolecular reactions of HOM-RO₂• with RO₂•, HO₂•
136 and NO lead to highly oxidized closed shell products including carbonyls, hydroperoxides, alcohols, or organic
137 nitrates as termination groups (R1 to R3), or form accretion products (R4) (Ehn et al., 2014; Mentel et al., 2015).
138 Unimolecular termination reactions of HOM-RO₂• lead to carbonyls or epoxides (R5 to R6) (Crouse et al., 2013).
139 On the other hand, reactions of HOM-RO₂• with NO, RO₂•, NO₃ at nighttime can lead to alkoxy radicals as chain

140 propagating steps (R7 to R9):



150 If the reactive HOM-RO• products undergo an H-migration reaction, they will again form HOM-RO₂ radicals
151 (“alkoxy-peroxy” pathway) (Mentel et al., 2015), continuing the autoxidation chain. Finally, the HOM-RO• may also
152 fragment leading to small RO₂ radicals, isomerize leading to carbonyls (Bianchi et al., 2019) or react with O₂ to form
153 carbonyls (Ziemann and Atkinson, 2012).

154 In this study, HOM formation in the NO₃ oxidation of limonene was investigated. We report the identification
155 of gas-phase HOM products, including monomers, dimers and trimers. The formation pathways of dominant products
156 in each category are proposed based on their time profiles in response to multiple additions of limonene in the
157 experiment and on the information in literature. Based on this analysis, we estimated HOM yields and discuss the
158 role of HOM in nucleation and growth of SOA particles.

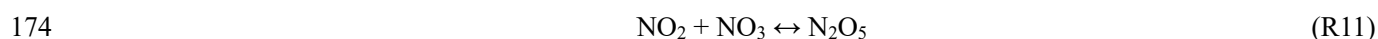
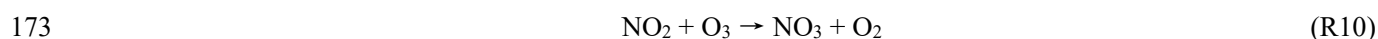
159

160 **2 Experimental and Methods**

161 **2.1 Experimental setup**

162 The limonene + NO₃ experiment was performed in the atmospheric simulation chamber SAPHIR (Simulation of
163 Atmospheric PHotochemistry In a large Reaction chamber) at the Forschungszentrum Jülich, Germany. SAPHIR is
164 a 270 m³ double-wall cylindrical Teflon chamber with a surface-to-volume ratio of ~1 m² m⁻³. Details of SAPHIR
165 have been described before (Rohrer et al., 2005; Zhao et al., 2015a; Zhao et al., 2015b; Zhao et al., 2018) and are
166 only summarized here. Detailed experimental procedures can be found in Fig. 1a. Before each experiment, SAPHIR
167 was flushed for about 4 h at a flow rate of 370 m³ h⁻¹ with high-purity synthetic air (purity >99.9999 % O₂ and N₂)
168 in order to clean the chamber. To simulate nighttime conditions for the NO₃ chemistry the chamber roof remained
169 closed throughout the experiment. The experiment was performed under dry conditions (RH <2 %) at a temperature
170 of 302 ± 3 K. No seed aerosols were used in the experiments. A fan was used for active mixing in the chamber,
171 leading to a typical mixing time of ~1 min (Fuchs et al., 2013).

172 NO₃ radicals were generated via the reaction of ozone with nitrogen dioxide:



175 Therefore, O₃ and NO₂ were first added to the chamber to form N₂O₅ and NO₃ with mixing ratios of ~2 ppbv
176 and ~0.15 ppbv, respectively. About 20 min later, 5 ppbv of limonene was added to start the organic chemistry. Five
177 more additions of limonene followed, with added concentrations of about 3 ppbv, 3 ppbv, 2 ppbv, 2 ppbv, and finally
178 8 ppbv, which divided the experiment into six periods (P1 to P6) (Fig. 1a). For period P3 and P5, NO₂ and O₃ were
179 also added to compensate for the loss of NO₃ and N₂O₅ (Fig. 1a). The concentrations of NO₂ and O₃ were maintained
180 around 20 to 70 ppbv throughout the experiment, ensuring the major loss of limonene was by reaction with NO₃
181 rather than with O₃ (Fig. S1 in the SI). In the first ten min of reaction (named period P1a hereafter, Fig. 1a), NO₃
182 accounted for 86 % of the chemical loss of limonene.

183 2.2 Instrumentation

184 Gas-phase HOM were detected by a Chemical Ionization time-of-flight Mass Spectrometer (CI-API-TOF, Aerodyne
185 Research Inc., USA) with a resolution (m/z)/($\Delta m/z$) of ~3800 using ¹⁵NO₃⁻ as the reagent ion, which is capable of
186 detecting organic molecules with high oxygen content (Eisele and Tanner, 1993; Jokinen et al., 2012). The mass
187 spectra were analyzed using the software Tofware (Tofwerk/Aerodyne) in Igor Pro (WaveMetrics, Inc.). Peak
188 identification was conducted by a high-resolution analysis (examples shown in Fig. S2). We observed several peaks
189 which were obviously products from the isoprene + NO₃ reaction, such as C₅H₁₀N₂O₈·¹⁵NO₃⁻ at m/z 289. Such peaks
190 were present before the limonene oxidation reaction started, suggesting that these compounds preexisted in the
191 chamber. These isoprene oxidation products were likely formed in an isoprene + NO₃ experiment performed two
192 days before (Zhao et al., 2021) and released slowly from chamber walls due to their semi-volatile character. Their
193 total concentration is less than 1 ppt. All the isoprene-HOM observed (C₅H₉NO_{7,10}, C₅H₈N₂O₈₋₁₀, C₅H₁₀N₂O₈,
194 C₅H₉N₃O_{9,10}) are saturated and do not contain C=C double bond. The isoprene-HOM will not influence the reaction
195 of limonene with NO₃ in this study. Therefore, they are not discussed as products from the limonene oxidation in our
196 experiment. (However, we cannot exclude that they were partly generated from fragmentation in the limonene + NO₃
197 reaction.)

198 A set of instruments were used to measure other gas-phase species, including VOC, NO_x, O₃, NO₃ and N₂O₅
199 (Shen et al., 2021). Concentrations of NO₃ and N₂O₅ were measured in-situ using a home-built diode laser-based,
200 cavity ring-down spectrometer similar to the instrument described in the work by Wagner et al. (2011). The
201 concentrations of limonene were measured using a Proton Transfer Reaction Time-of-Flight Mass Spectrometer
202 (PTR-TOF-MS, Ionicon Analytik, Austria). The SOA number concentration, surface concentration and size
203 distribution were detected by an SMPS (TSI DMA3081/TSI CPC3786) and a CPC (TSI 3785). Temperature and
204 relative humidity were continuously monitored throughout the experiment.

205 2.3 Determination of HOM concentration and “primary” HOM yield

206 HOM concentrations were obtained from the normalized signals to the total signals of the mass spectra (nc ,
207 normalized counts) by applying a calibration coefficient (C) of 2.5×10^{10} molecule $cm^{-3} nc^{-1}$. C was determined using
208 H₂SO₄ as the charging efficiency of HOM and H₂SO₄ are considered to be equal (Ehn et al., 2014; Pullinen et al.,
209 2020; Shen et al., 2021). The details of determination of the calibration coefficient are shown in the supplement S1.

210 A mass-independent transmission efficiency was used according to our previous study, which causes an additional
 211 uncertainty of 14 % (Pullinen et al., 2020). In this previous study, the transmission efficiency curve of nitrate CI-API-
 212 TOF was determined and found to monotonously decrease with increasing mass of ions but only slightly depend on
 213 the mass range (14 % change). As we used the same setting as our previous study, we have included the slight
 214 dependence of transmission on m/z in the uncertainties. The concentrations of HOM were corrected for chamber wall
 215 losses, which were determined for a number of HOM similar to our previous study (Zhao et al., 2018), with details
 216 described in the supplement. When the chamber is actively mixed, the wall loss was determined to be $(2.2 \pm 0.2) \times 10^{-3}$
 217 s^{-1} . As the HOM yield was determined during the first 3 min of the experiment, we considered the wall loss rate to
 218 be constant ($2.2 \times 10^{-3} s^{-1}$) during this period. Sensitivity analysis showed that the HOM yield in this study is not very
 219 sensitive to the wall loss rate and is changing by only +0.88 % and -0.44 % if the wall loss rate is varied by +100 %
 220 or -50 %.

221 The HOM yield was calculated as:

$$222 \quad Y = \frac{[HOM]}{[VOC]_r} = \frac{I(HOM) \cdot C}{[N_2O_5]_r} \quad (\text{Eq. 1})$$

223 where $[HOM]$ is the concentration of HOM, $I(HOM)$ is the total signal intensity of HOM, C is the calibration factor,
 224 and $[VOC]_r$ and $[N_2O_5]_r$ stand for the concentrations of limonene and N_2O_5 reacted, respectively. We used the
 225 reacted concentration of N_2O_5 rather than the measured reacted limonene concentration as a large fraction of limonene
 226 was already reacting away during the VOC injection before it was homogeneously mixed in the chamber. During this
 227 part of the experiment, the high limonene concentration resulted in a rapid loss of NO_3 , such that every NO_3 formed
 228 from the decomposition of N_2O_5 reacted with limonene:



231 The initial NO_3 concentration before the limonene injection was small compared to the time-integrated loss of N_2O_5 ,
 232 and other NO_3 loss processes were negligible right after the limonene injection, so that the observed decrease in the
 233 N_2O_5 concentration equals indeed the consumption of limonene. The wall loss rate constant of N_2O_5 in the SAPHIR
 234 chamber is $7.2 \times 10^{-5} s^{-1}$ (Fry et al., 2009). As the HOM yield determination is based on the first 3 min, the wall loss
 235 of N_2O_5 can be ignored compared to the loss via the reaction of NO_3 with limonene.

236 The uncertainty of the HOM yield was estimated to be -55 %/ +117 % based on the combined uncertainties of
 237 the HOM-ON peak intensities (~10 %), the limonene concentration (~15 %), the transmission efficiency (-0 %/+14 %)
 238 and the calibration factor (-52 %/ +101 %) using error propagation (Zhao et al., 2021). The first 3 min after the
 239 injection of limonene were used to calculate the HOM yield, when most of the first-generation oxidation products
 240 were produced and negligible particles were yet formed. The HOM yield thus reflects the “primary” HOM yield.

241 **2.4 Determination of HOM condensation on SOA**

242 The SOA mass from the condensation of HOM was calculated to evaluate the role of HOM for the SOA mass growth.
 243 Detailed estimation methods are described in the supplement, including the determination of particle wall loss and
 244 dilution loss rate (Sect. S2). In brief, the growth rate of SOA through HOM vapor condensation is based on the

245 collision rate of vapor molecules with aerosols in the kinetic regime. The Fuchs-Sutugin approach is applied to
246 describe the correction for transition from the kinetic to the diffusion regime (Fuchs and Sutugin, 1971; Ehn et al.,
247 2014). Based on the volatility of HOM, we considered two scenarios for HOM condensation. In Scenario 1, all HOM
248 were assumed to irreversibly condense on the surface of particles leading to particle mass growth. In Scenario 2, only
249 the irreversible uptake of LVOC and ULVOC/ELVOC compounds were considered to contribute to the growth of
250 SOA particles in order to examine the role of LVOC and ELVOC while IVOC and SVOC were not included, although
251 they may also contribute to SOA. The calculation of saturation concentration C^* (in $\mu\text{g}/\text{m}^3$) of each HOM was done
252 based on their molecular compositions using two different parameterizations considering the uncertainties in
253 estimating volatility (Wu et al., 2021b):

254 1. an updated version of the parameterization of Donahue et al. (2011) by Mohr et al. (2019) (Scenario 2a):

$$255 \log_{10}(C) = (25 - n_C) \times 0.475 - (n_O - 3n_N) \times 0.2 - 2 \frac{(n_O - 3n_N)n_C}{(n_C + n_O - 3n_N)} \times 0.9 - n_N \times 2.5 \quad (\text{Eq. 2})$$

256 where n_C , n_O , n_N and n_H are the number of carbon, oxygen, nitrogen and hydrogen atoms of the compound,
257 respectively.

258 2. a parameterization based on HOM from α -pinene ozonolysis by Peräkylä et al. (2020) (Scenario 2b):

$$259 \log_{10}(C) = n_C \times 0.18 - n_H \times 0.14 - n_O \times 0.38 + n_N \times 0.80 + 3.1 \quad (\text{Eq. 3})$$

260 with similar parameter notation.

261 **2.5 Simulations of the RO₂• loss pathway based on the Master Chemical Mechanism (MCM)**

262 The RO₂• loss pathways were estimated based on MCM simulations (<http://mcm.york.ac.uk/>). The gas-phase
263 reactions of limonene + NO₃ under dark condition were simulated using iChamber, an open-source program
264 (<https://sites.google.com/view/wangsiyuan/models?authuser=0>) (Wang and Pratt, 2017). The default chemistry of
265 limonene + NO₃ in the MCM was applied in this study (Saunders et al., 2003b). Photolysis reactions were excluded
266 by setting the zenith angle to 90°. Concentrations of O₃, NO₃, NO₂ and N₂O₅ as well as temperature and relative
267 humidity were constrained to the experimental data with a time resolution of 1 min. The chamber dilution rate of
268 $1.5 \times 10^{-5} \text{ s}^{-1}$ was applied to all species. The P1 period was simulated using the above conditions and the initial
269 concentrations of limonene were added in the model according to the experimental procedures. The sum of all 140
270 RO₂• in the limonene subset of MCM v3.3.1 were used in the usual way to estimate the loss rates of RO₂• bimolecular
271 reactions. The reaction rate constants are provided in Table S3, and calculated loss rates are shown in Fig. S3. We
272 note that the MCM reaction schemes do not include the accretion reactions between HOM-RO₂•. Berndt et al. (2018a)
273 determined the rate constant of accretion reaction of C₁₀H₁₅O₄• formed via α -pinene ozonolysis to be $\sim 1 \times 10^{-11} \text{ cm}^3$
274 $\text{molecule}^{-1} \text{ s}^{-1}$, which is of the same order as the upper limit for RO₂• + RO₂• reactions used in the MCM schemes
275 for functionalized peroxy radicals such as acyl peroxy radicals (Jenkin et al., 1997; Saunders et al., 2003a). However,
276 currently we do not see a reliable updated set of rate coefficients that are applicable to the reaction system in this
277 study. If the rate constants of some RO₂• + RO₂• reactions were higher than those used in MCM, the concentrations
278 of RO₂• would be lower and relative importance of RO₂• + RO₂• in RO₂• fate would increase. Several simulation
279 results are shown in Fig. S4, including NO₃, N₂O₅, limonene, RO₂•, reaction rate of limonene with NO₃

280 ($k \times \text{limonene} \times \text{NO}_3$), and examples of 1st and 2nd-generation $\text{RO}_2\bullet$.

281 In the early stage of each period, $\text{RO}_2\bullet$ mainly reacted with $\text{RO}_2\bullet$ and NO_3 , although in the later stage the reaction
282 with NO_2 also contributed to a significant fraction of $\text{RO}_2\bullet$ loss (Fig. S3, showing period P1 as an example). During
283 the period P1a when our peak assignment was based on, the $\text{RO}_2\bullet$ loss was dominated by $\text{RO}_2\bullet + \text{RO}_2\bullet$ and $\text{RO}_2\bullet +$
284 NO_3 .

285

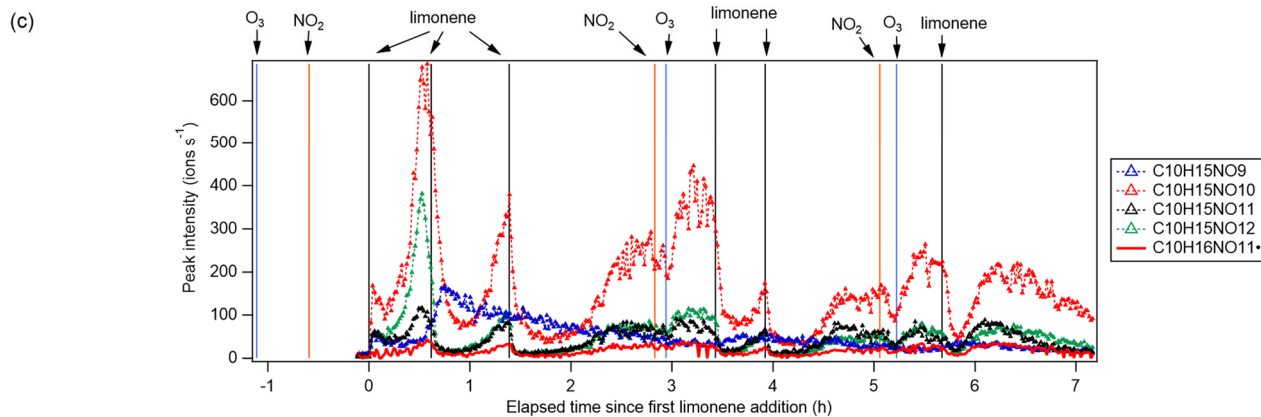
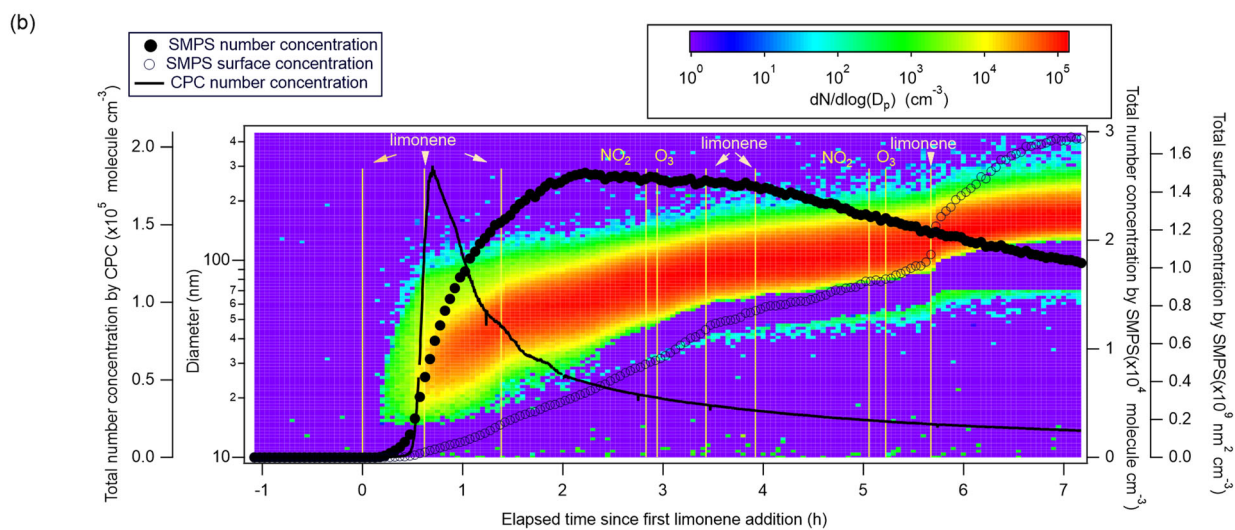
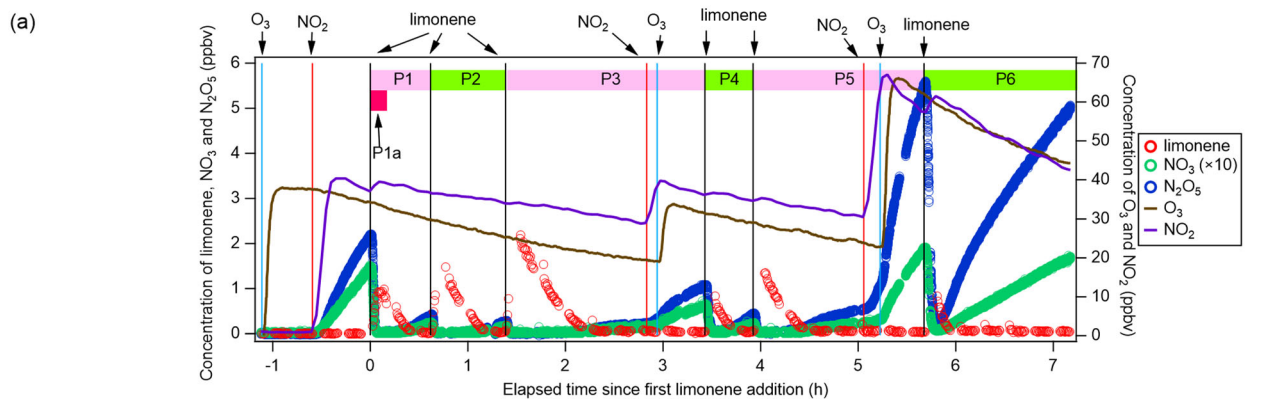
286 **3 Results and discussion**

287 **3.1 Experiment overview and observed HOM**

288 After each limonene addition, the concentration of limonene rose first and then rapidly declined, while the
289 concentrations of NO_3 and N_2O_5 rapidly decreased due to the fast reaction between limonene and NO_3 and gradually
290 increased when limonene had been consumed (Fig. 1a). About 10 min after the first limonene addition, new particles
291 had already formed and quickly grew in size (Fig. 1b). Therefore, we used the first 10 min reaction time (period P1a)
292 to identify gas-phase HOM products, and the whole experiment to examine the contribution of HOM to SOA.

293 During period P1, HOM were quickly formed. We identified about 280 HOM compounds, including monomers
294 ($\text{C}_7\text{-C}_{10}$, ~280-460 Th), dimers ($\text{C}_{17}\text{-C}_{20}$, ~490-700 Th), and trimers ($\text{C}_{26}\text{-C}_{30}$, ~720-960 Th) (Fig. 2a). Their detailed
295 formulas can be found in Table S1. HOM on the horizontal lines of the Kendrick mass defect plot (O-based) (Fig. 3
296 and Fig S5, S6) share the same number of C, N and H atoms, with the number of oxygen atoms increasing from left
297 to right. Such HOM compounds are defined as a family. We notice that most monomer peroxy radical families are
298 each related to two monomer closed-shell product families, with one H atom more or one H atom less, which are the
299 expected termination products of $\text{RO}_2\bullet + \text{RO}_2\bullet$ reactions, or if $\text{HO}_2\bullet$ is present, $\text{RO}_2\bullet + \text{HO}_2\bullet$ termination products.
300 These three related families are defined as a "series", with the same number of C and N number, such as $\text{C}_{10}\text{H}_{15-}$
301 $_{17}\text{NO}_{6-14}$. In total, we identified 6 monomer series ($\text{C}_{10}\text{H}_{15-17}\text{NO}_{6-14}$, $\text{C}_{10}\text{H}_{14-16}\text{N}_2\text{O}_{9-15}$, $\text{C}_{10}\text{H}_{14-16}\text{O}_{7-12}$, $\text{C}_9\text{H}_{13-15}\text{NO}_{7-14}$,
302 $\text{C}_8\text{H}_{11-13}\text{NO}_{6-13}$ and $\text{C}_7\text{H}_{9-11}\text{NO}_{7-11}$) and 1 monomer family ($\text{C}_{10}\text{H}_{17}\text{N}_3\text{O}_{12-16}$), 11 dimer families ($\text{C}_{20}\text{H}_{31}\text{NO}_{10-15}$,
303 $\text{C}_{20}\text{H}_{33}\text{NO}_{12-16}$, $\text{C}_{20}\text{H}_{32}\text{N}_2\text{O}_{9-20}$, $\text{C}_{20}\text{H}_{31}\text{N}_3\text{O}_{14-20}$, $\text{C}_{20}\text{H}_{33}\text{N}_3\text{O}_{12-20}$, $\text{C}_{20}\text{H}_{34}\text{N}_4\text{O}_{15-20}$, $\text{C}_{20}\text{H}_{32}\text{O}_{13-16}$, $\text{C}_{19}\text{H}_{29}\text{NO}_{10-13}$,
304 $\text{C}_{19}\text{H}_{31}\text{NO}_{10-15}$, $\text{C}_{19}\text{H}_{30}\text{N}_2\text{O}_{10-18}$ and $\text{C}_{19}\text{H}_{31}\text{N}_3\text{O}_{15-19}$), and 3 trimer families ($\text{C}_{30}\text{H}_{47}\text{N}_3\text{O}_{18-24}$, $\text{C}_{30}\text{H}_{48}\text{N}_4\text{O}_{16-24}$ and
305 $\text{C}_{29}\text{H}_{46}\text{N}_4\text{O}_{19-24}$). The monomer family $\text{C}_{10}\text{H}_{17}\text{N}_3\text{O}_{12-16}$ are not classified as series because the supposedly relevant
306 families are not clearly identified. Compounds containing at least one nitrogen atom accounted for more than 90 %
307 of the identified HOM products. We assume that compounds containing nitrogen atoms are organic nitrates, because
308 other N-containing species such as amines or nitro compounds are very unlikely to be formed from the reaction of
309 limonene with NO_3 . Organic nitrates formed in this study could be alkyl nitrates, or (acyl)peroxynitrates formed via
310 the reaction of $\text{RO}_2\bullet$ with NO_2 .

311 During period P1a, in the absence of particles, both HOM monomers and oligomers were observed, including
312 monomers (47 %), dimers (47 %) and trimers (6 %) (Fig. 2a). Concentrations of gas-phase dimers and trimers
313 decreased evidently after particle formation (Fig. 2b, 5, 6), indicating a fast gas-particle condensation and strong
314 tendency of oligomers to condense on particles.



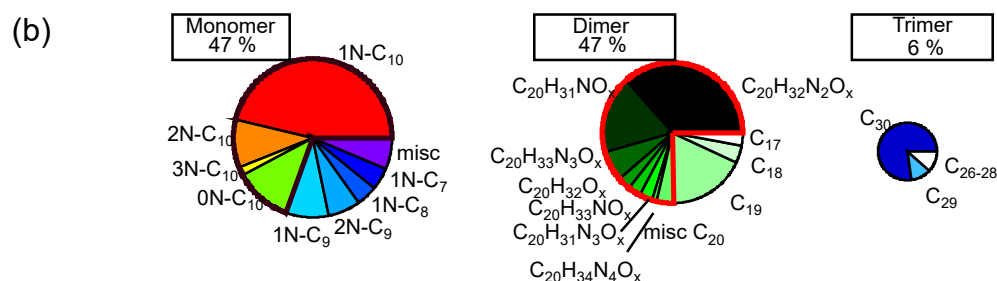
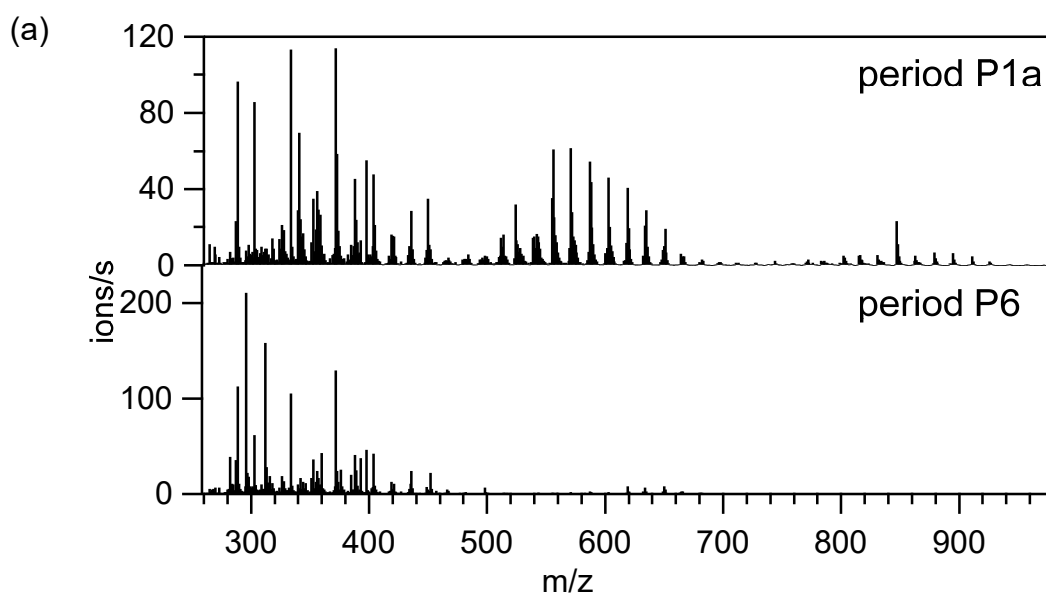
315
 316 Figure 1. (a) Time series of the concentrations of limonene, NO_3 , N_2O_5 (left panel, the concentrations of NO_3 are
 317 magnified by a factor of 10 for clarity), as well as O_3 and NO_2 (right panel). The time periods P1 to P6 as well as
 318 P1a are also marked. (b) Total particle concentration and its size distribution during the whole period of experiment
 319 detected by SMPS and CPC. The solid and hollow black circles refer to total number concentration and total
 320 surface concentration detected by SMPS, respectively. Colors represent particle number concentration distribution
 321 based on $\log(D_p)$. The solid black line refers to total number concentration detected by CPC. (c) Time series of peak
 322 intensity of typical products of the $\text{C}_{10}\text{H}_{15}\text{NO}_x$ family and $\text{C}_{10}\text{H}_{16}\text{NO}_{11}\bullet$ as a representative of the $\text{C}_{10}\text{H}_{16}\text{NO}_x\bullet$

323 family. Vertical lines indicate the time of O₃ and NO₂ additions, as well as six limonene injections.

324

325 Based on their typical time series (Fig. 1c), products can be classified as first-generation or second-generation
326 products. Generally, the concentrations of first-generation products, which result from the direct reaction of limonene
327 with NO₃, are expected to quickly increase after the limonene addition, followed by a steady decline due to wall loss
328 or chemical reactions. Concentrations of typical second-generation products, which result from further reactions of
329 first-generation products, are expected to show a gradually increasing concentration pattern after a limonene addition
330 and reach their maximum concentration later than first-generation products. These general expectations are modified
331 in our case, since the particle concentration increased in our experiment (Fig. 1b) and the condensational sink of
332 HOM products became stronger over time. Thus, an increase in concentration suggests that the increasing
333 condensational sink was exceeded by increasing production with time, i.e. from second-generation pathways.

334 To sum up, gas-phase HOM formed in the limonene + NO₃ system were dominated by HOM monomers and
335 dimers. Time series patterns of the products indicate multiple generations of reaction pathways.



336

337 Figure 2. (a) Average mass spectra of the first 10 min reaction time after the first addition of limonene (period P1a,
338 upper panel) and the last limonene addition period till particles reached maximum mass concentration (period P6,

339 lower panel). (b) Pie charts (from left to right: rainbow, green, and blue colors) representing the relative contributions
 340 of identified families to HOM monomers, dimers, and trimers, respectively, during the P1a period. The area of each
 341 pie is in proportion to their concentrations during the P1a period.

342

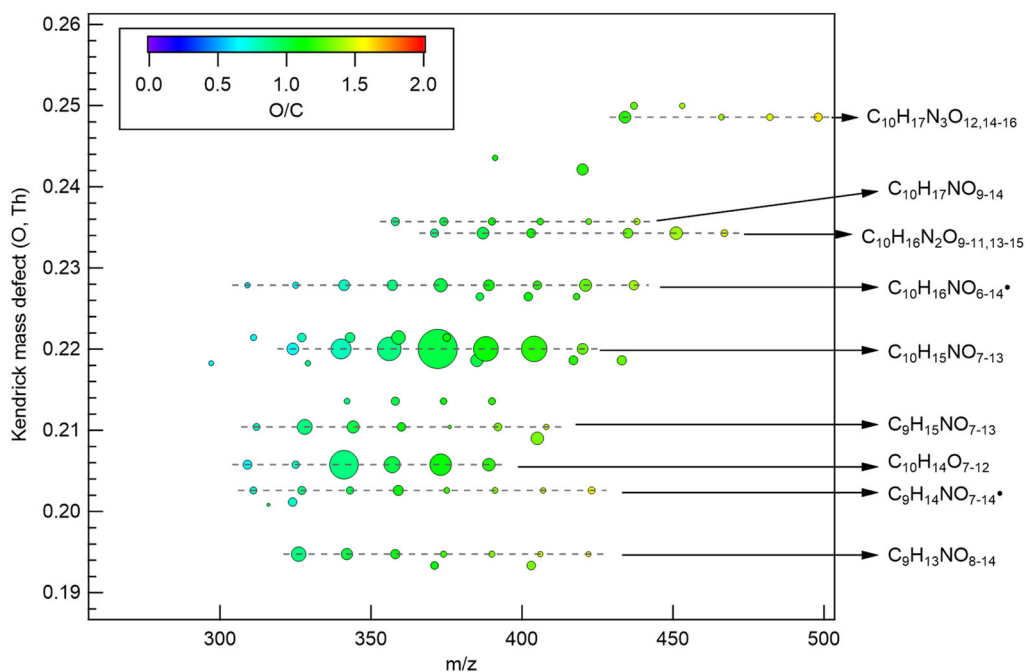
343 3.2 Monomers and their formation pathways

344 3.2.1 Overview of HOM monomers

345 A number of HOM monomer families were detected with an increasing oxygenation pattern at 16 Th intervals (Fig.
 346 3). Such a pattern is attributed to autoxidation of RO_2^\bullet (with 32 Th interval for each O_2 addition) plus the alkoxy-
 347 peroxy pathway (shifted by 16 Th compared with exclusive autoxidation) as discussed below. During period P1a, the
 348 most abundant HOM monomers are C_{10} compounds (64 %), such as peroxy radicals $\text{C}_{10}\text{H}_{16}\text{NO}_x^\bullet$ and closed-shell
 349 products $\text{C}_{10}\text{H}_{15}\text{NO}_x$ and $\text{C}_{10}\text{H}_{17}\text{NO}_x$, which are carbonyl compounds and hydroxyl or hydroperoxy compounds from
 350 the termination reactions of $\text{C}_{10}\text{H}_{16}\text{NO}_x^\bullet$, respectively (R14).



352 According to the nitrogen atoms contained, C_{10} -HOM monomers can be classified into 1N-, 2N-, 3N-monomers,
 353 and monomers without nitrogen atoms. While 1N- C_{10} HOM monomers were likely formed by direct NO_3 addition
 354 to limonene, C_{10} HOM monomers containing multiple N atoms were likely formed via multiple reaction steps.
 355 Besides C_{10} HOM monomers, C_{6-9} HOM monomers were also observed. These C_{6-10} families are discussed below in
 356 the order of their contributions to HOM monomers.



357

358 Figure 3. Kendrick mass defect plot (O-atom-based) of major monomer products. The area of the circles is
 359 proportional to the average intensity of each compound during the P1a period with the largest circle representing
 360 $\text{C}_{10}\text{H}_{15}\text{NO}_{10}$. The color denotes O/C ratios. Dashed lines indicate major product families. For clarity, the reagent ions

361 $^{15}\text{NO}_3^-$ is omitted from molecular formula. The calculation of O-atom-based Kendrick mass defect includes two steps.
362 First, the IUPAC mass scale (based on the ^{12}C atomic mass as exactly 12 Da) is rescaled to Kendrick mass: Kendrick
363 mass = IUPAC mass \times (16/15.9949), which converts the mass of O from 15.9949 to exactly 16. Then, Kendrick mass
364 defect is given by: Kendrick mass defect = nominal Kendrick mass – exact Kendrick mass. Thus, compounds with
365 the same number of each kind of atom except for O have equal O-atom-based Kendrick mass defect, and are shown
366 in a horizontal line in the O-atom-based Kendrick mass defect plot.

367

368 3.2.2 1N-C₁₀ monomers

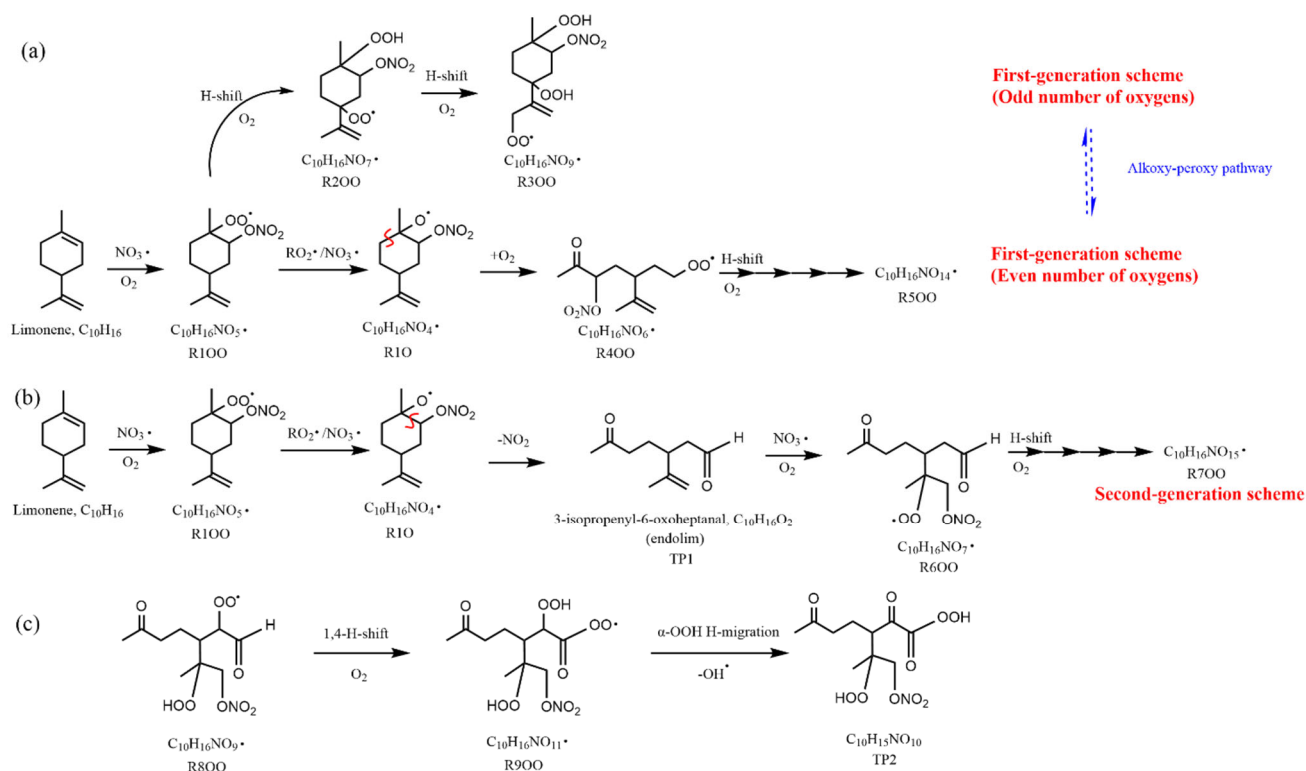
369 Among C₁₀ HOM monomers, the 1N-C₁₀ families were most abundant and included stable closed-shell products
370 C₁₀H₁₅NO_x (x=7-13) and C₁₀H₁₇NO_x (x=9-14) and peroxy radicals C₁₀H₁₆NO_x• (x=6-14). The concentration of
371 C₁₀H₁₆NO₁₁• increased in the later phase of each limonene addition period (Fig. 1c), showing mostly a time profile
372 of a second-generation product, similar as most of the other radicals in the C₁₀H₁₆NO_x• family (Fig. S7). However,
373 the time series of C₁₀H₁₅NO_x compounds showed an overlaying pattern of first- and second-generation products
374 dominated by a second-generation time profile with the exception of C₁₀H₁₅NO₉ (Fig. 1c). Due to sensitivity
375 restrictions of CIMS, the primary peroxy radical C₁₀H₁₆NO₅• was not detected, which was supposed to show 1st-
376 generation pattern. The absence of first-generation characteristics of the time profile of most HOM peroxy radicals
377 C₁₀H₁₆NO_{x(x≥6)}• may be attributed to two possible reasons. They either did not undergo efficient autoxidation, or they
378 underwent immediate conversion including autoxidation and/or bimolecular reactions with other RO₂• or NO₃
379 forming closed-shell products such as dimers or continuing the radical chain forming RO•. The instantaneous increase
380 of 2N-dimers and trimers after the first limonene addition shown below suggests that C₁₀H₁₆NO_{x(x≥6)}• were indeed
381 formed efficiently via autoxidation. Therefore, the latter reason is more likely. At this time, we do not have a
382 reasonable explanation for the trend of C₁₀H₁₅NO₉, though we should consider that there are many isomers at play,
383 which may have very different chemical pathways (un)available.

384 Since the C₁₀H₁₅NO_x family showed an overlaying pattern of the first-generation and second-generation
385 products, they likely contained multiple isobaric substances produced through different pathways. Based on the
386 literature, possible formation pathways of these products were tentatively proposed (Seinfeld and Pandis, 2006;
387 Vereecken and Peeters, 2010; Mentel et al., 2015; Vereecken and Nozière, 2020). As an example of the pathways to
388 form first-generation products, C₁₀H₁₆NO_{2x-1}• (with an odd number of oxygen atom) and their corresponding
389 termination products can be formed via autoxidation of the first peroxy radical C₁₀H₁₆NO₅• (R1OO), showing
390 C₁₀H₁₆NO₉• (R3OO) as an example (Scheme 1a, first-generation products). C₁₀H₁₆NO_{2x}• (with an even number of
391 oxygen atom) can be formed via alkoxy-peroxy channels. For example, the ring-opening of the alkoxy radical
392 C₁₀H₁₆NO₄• (R1O), which was formed via the reaction of C₁₀H₁₆NO₅• (R1OO) with another RO₂• or NO₃ radical
393 (Scheme 1a, first-generation products). Ring-opening of R1O leads to C₁₀H₁₆NO₆• (R4OO), which can undergo
394 autoxidation forming C₁₀H₁₆NO_{2x}•. In addition, the alkoxy radical C₁₀H₁₆NO₄• (R1O) is susceptible to ring-opening
395 reactions (Novelli et al., 2021), which can lead to a first-generation stable product 3-isopropenyl-6-oxoheptanal

396 (endolim, TP1) after C-C bond cleavage followed by the elimination of a NO₂ fragment (Scheme 1b, second-
 397 generation products). Endolim (TP1) has been detected as a major product in previous limonene + NO₃ studies
 398 (Hallquist et al., 1999; Spittler et al., 2006).

399 As an example of second-generation chemistry, the remaining double bond of endolim could react with NO₃ to
 400 form RO₂•, followed by the autoxidation to form second-generation C₁₀H₁₆NO_x• (with odd number of oxygen atoms).
 401 Similar to first-generation pathways, second-generation C₁₀H₁₆NO_x• with even number of oxygen atoms can be
 402 formed via alkoxy-peroxy channel. From the time profile of C₁₀H₁₅NO_x, the second-generation pathway (Scheme 1b)
 403 was expected to play a more important role, in agreement with the theoretical result by Kurtén et al. (2017), in which
 404 the two bond-cleavage pathways of limonene-derived RO• radical were considered. It is worth mentioning that the
 405 reaction products of limonene with O₃ may also react with NO₃, forming C₁₀H₁₆NO_x• (Scheme S1). However, as
 406 shown above, this was a minor pathway in our experiment (Sect. 2.1). We would like to note that to simplify the
 407 scheme, only the reaction of NO₃ with the endocyclic double bond is presented, since this reaction is faster than that
 408 with the exocyclic double bond (Jiang et al., 2009; Fry et al., 2011).

409 C₁₀H₁₆NO_x• with both even and odd number of oxygen atoms as well as their termination products had
 410 comparable abundance, which suggests that the alkoxy-peroxy pathway was important for RO₂• formation in this
 411 reaction. This finding is analogous to the findings in the reaction of a number of alkenes with O₃ and in the reaction
 412 of isoprene and β-pinene with NO₃ (Mentel et al., 2015; Zhao et al., 2021; Shen et al., 2021).



413
 414 Scheme 1. Illustrative scheme for HOM formation in the limonene + NO₃ reaction. (a) Example formation pathways
 415 leading to first-generation 1N-C₁₀ HOM-RO₂ radicals (C₁₀H₁₆NO_x• with even or odd numbers of O-atoms). (b)
 416 Second-generation scheme involving the formation of endolim. (c) Scheme of intramolecular termination of RO₂•

417 radicals forming carbonyl products taking the $C_{10}H_{16}NO_9\bullet$ radical as an example. Note that the depicted reactions
418 may not be the dominant pathways.

419

420 Among 1N- C_{10} monomers, concentrations of carbonyl compounds were much higher than the sum of hydroxy-
421 and hydroperoxy-substituted compounds (Table 1). According to Hyttinen et al. (2015), for nitrate CI-API-TOF,
422 HOM containing two hydrogen bond donors (such as -OOH and -OH group) have strong binding energy with NO_3^- .
423 Additional hydrogen bond donors only enhance the binding energy marginally. If we compare HOM carbonyl product
424 (such as $C_{10}H_{15}NO_{10}$) with the corresponding hydroxy product ($C_{10}H_{17}NO_{10}$), they only differ in one functional group.
425 As both are highly functionalized, it is likely that HOM carbonyl have a quite similar sensitivity with HOM alcohol.
426 If the sensitivity of carbonyl HOM were lower, this would result in even more dominance of carbonyl HOM over
427 hydroxyl HOM. Thus, we conclude that carbonylnitrates are more abundant than hydroxynitrates or
428 hydroperoxynitrates. This finding is likely attributed to unimolecular termination reactions of $RO_2\bullet$, although reaction
429 paths via $RO\bullet$ also cannot be excluded. Smaller unbranched $RO\bullet$ tend to react with O_2 forming carbonyl compounds
430 while for larger or branched $RO\bullet$, isomerization can also form carbonyl compounds and is a more energetically
431 favorable and thus faster pathway compared with the reaction with O_2 (Ziemann and Atkinson, 2012). The importance
432 of unimolecular termination reactions of $HOM-RO_2\bullet$ and the resulting high ratio of carbonyl compounds to
433 hydroxyl/hydroperoxyl compounds has also been found in the reaction system of β -pinene + NO_3 (Shen et al., 2021;
434 Dam et al., 2022). This high ratio is also consistent with findings in the ozonolysis of alkenes (Mentel et al., 2015),
435 where unimolecular termination reactions were also proposed to be the likely explanation (Crouse et al., 2013;
436 Rissanen et al., 2014). As discussed in our previous study by Shen et al. (2021), this higher abundance of
437 carbonylnitrates is not likely to be explained by the reaction of alkoxy $RO\bullet + O_2$ forming carbonyls and $HO_2\bullet$,
438 decomposition of β -nitrooxyperoxynitrate or self-reactions of $RO_2\bullet$ via the Bennett and Summers mechanism forming
439 carbonyls and H_2O_2 . Reactions between $RO_2\bullet$ in general should produce overall equal amounts of carbonyl and
440 hydroxyl compounds. The decomposition of β -nitrooxyperoxynitrate is slow in the gas-phase. The reaction of alkoxy
441 $RO\bullet$ with O_2 for large $RO\bullet$ is generally slower than isomerization and decomposition (Vereecken and Peeters, 2009,
442 2010). Thus, the higher abundance of carbonylnitrates compared to hydroxynitrates may be attributed to unimolecular
443 termination of $HOM-RO_2\bullet$. In addition, isomerization of $RO\bullet$ forming carbonyl compounds may also contribute to
444 this finding. Our result thus further emphasizes that unimolecular termination reactions of RO_2 radicals are important
445 pathways in the formation of HOM monomers derived from the reactions of monoterpenes with NO_3 (Shen et al.,
446 2021). Scheme 1c shows this unimolecular termination process using a $C_{10}H_{16}NO_9\bullet$ radical as an example.
447 $C_{10}H_{16}NO_9\bullet$ undergoes a 1,4-H-shift and O_2 addition to form a $C_{10}H_{16}NO_{11}\bullet$ radical. The $C_{10}H_{16}NO_{11}\bullet$ radical further
448 undergoes an H-shift of the α -OOH H-atom, which produces a carbonyl closed-shell product as well as an $OH\bullet$
449 radical.

450 For 1N- C_{10} HOM monomers, the products detected in this study generally agree with previous laboratory and
451 field studies on the reaction of limonene and other monoterpenes. Faxon et al. (2018) also observed $C_{10}H_{15}NO_x$ as

452 the most prevalent products in the particle phase from limonene + NO₃. In the SOAS campaign, both C₁₀H₁₅NO_x and
 453 C₁₀H₁₇NO_x products were detected and were believed to be products of nighttime chemistry (Lee et al., 2016). The
 454 high abundance of 1N-C₁₀ HOM monomers is consistent with the finding that C₁₀H₁₅NO_x and C₁₀H₁₇NO_x dominate
 455 the chemical composition of SOA formed via NO₃ oxidation of α-pinene and β-pinene, as shown in previous chamber
 456 studies (Takeuchi and Ng, 2019).

457 In summary, 1N-C₁₀ HOM monomers are mainly formed via second-generation pathways, and unimolecular
 458 termination of RO₂• likely plays an important role leading to higher abundance of carbonyl HOM-ON (C₁₀H₁₅NO_x)
 459 than hydroxy/hydroperoxy HOM-ON (C₁₀H₁₇NO_x).

460

461 Table 1. Observed C₁₀H₁₆NO_x• radicals (m) and their termination products, including carbonyl compounds (m-17),
 462 hydroxyl compounds (m-15), and hydroperoxy compounds (m+1). Their concentrations during period P1a are
 463 normalized to that of C₁₀H₁₅NO₁₀, which had the highest concentration among the families of 1N-C₁₀ monomers.
 464 Their relative signal intensities during the P1a period are shown in the second line of each cell.

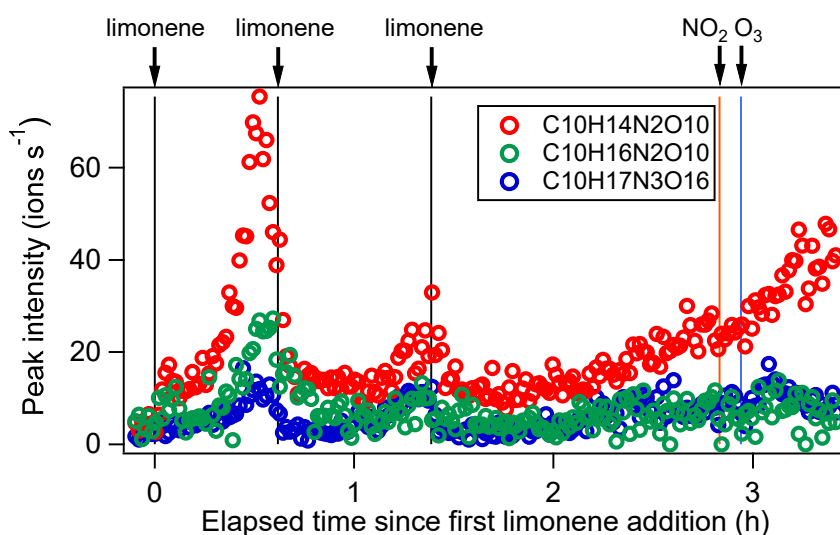
Peroxy radical m	Carbonyl m-17	Hydroxy m-15	Hydroperoxy m+1
C ₁₀ H ₁₆ NO ₆ • 1.5 %			
C ₁₀ H ₁₆ NO ₇ • 2.0 %			
C ₁₀ H ₁₆ NO ₈ • 6.7 %	C ₁₀ H ₁₅ NO ₇ 8.0 %		
C ₁₀ H ₁₆ NO ₉ • 6.0 %	C ₁₀ H ₁₅ NO ₈ 25.2 %		C ₁₀ H ₁₇ NO ₉ 3.7 %
C ₁₀ H ₁₆ NO ₁₀ • 10.2 %	C ₁₀ H ₁₅ NO ₉ 34.6 %	C ₁₀ H ₁₇ NO ₉ 3.7 %	C ₁₀ H ₁₇ NO ₁₀ 3.6 %
C ₁₀ H ₁₆ NO ₁₁ • 6.6 %	C ₁₀ H ₁₅ NO ₁₀ 100.0 %	C ₁₀ H ₁₇ NO ₁₀ 3.6 %	C ₁₀ H ₁₇ NO ₁₁ 3.0 %
C ₁₀ H ₁₆ NO ₁₂ • 4.1 %	C ₁₀ H ₁₅ NO ₁₁ 39.0 %	C ₁₀ H ₁₇ NO ₁₁ 3.0 %	C ₁₀ H ₁₇ NO ₁₂ 2.3 %
	C ₁₀ H ₁₅ NO ₁₂ 41.2 %	C ₁₀ H ₁₇ NO ₁₂ 2.3 %	C ₁₀ H ₁₇ NO ₁₃ 1.5 %
C ₁₀ H ₁₆ NO ₁₄ • 4.7 %	C ₁₀ H ₁₅ NO ₁₃ 6.7 %	C ₁₀ H ₁₇ NO ₁₃ 1.5 %	C ₁₀ H ₁₇ NO ₁₄ 1.8 %
		C ₁₀ H ₁₇ NO ₁₄ 1.8 %	

465

466 3.2.3 2N and 3N-C₁₀ monomers

467 C₁₀ monomers with 2 and 3 nitrogen atoms accounted for 27 % and 1 % of HOM monomers, respectively. They were
 468 likely formed via the reaction of a second attack of NO₃ to the first-generation products as the 1N-C₁₀ closed-shell

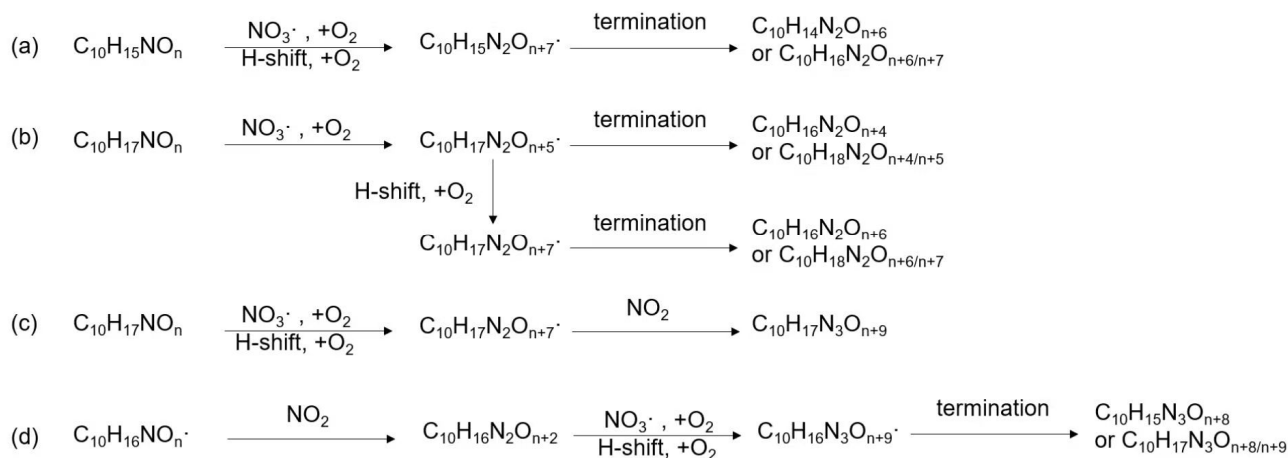
469 products formed via the reactions shown in Scheme 1a should contain a remaining limonene C=C double bond.
 470 Typical 2N- and 3N-HOM showed a second-generation time profile (Fig. 4). For clarity, only periods P1 to P3 are
 471 shown. This time profile is consistent with the pathways with multiple NO₃ attacks. Scheme 2 shows possible
 472 formation pathways of 2N- and 3N-C₁₀ monomers. 2N-C₁₀ HOM were likely to be formed from NO₃ oxidation of
 473 1N-C₁₀ monomers (C₁₀H₁₅NO_x and C₁₀H₁₇NO_x), resulting in C₁₀H₁₅N₂O_x• and C₁₀H₁₇N₂O_x• (Scheme 2a, 2b). While
 474 C₁₀H₁₅N₂O_x• (x=9-12) were observed, C₁₀H₁₇N₂O_x• could not be uniquely identified because the peaks of the
 475 C₁₀H₁₇N₂O_x• and C₁₀H₁₅NO_x families are too close in the mass spectra to be separated based on the resolution of our
 476 mass spectrometer. 3N-C₁₀ monomers, C₁₀H₁₇N₃O_x, were expected to be formed from limonene via two steps of NO₃
 477 oxidation to the double bonds and an addition of NO₂ to an RO₂ radical, leading to a peroxyacynitrate or
 478 peroxyacylnitrate. NO₂ addition reactions may also contribute to the formation of 2N-C₁₀ monomers. The addition
 479 of NO₂ to RO₂ radicals could occur either before (Scheme 2d) or after (Scheme 2c) the second NO₃ attack.



480

481 Figure 4. Time series of peak intensity of several monomers C₁₀H₁₄N₂O₁₀, C₁₀H₁₆N₂O₁₀ and C₁₀H₁₇N₃O₁₆ as the
 482 representatives of multiple N monomers during the periods P1-P3.

483



484

485 Scheme 2. Possible formation pathways of C₁₀-monomers containing 2 nitrogen atoms (a, b) and 3 nitrogen atoms

486 (c, d). Termination denotes reactions of $\text{RO}_2\bullet$ with other $\text{RO}_2\bullet$ or HO_2 , or unimolecular reactions, leading to closed-
487 shell products.

488

489 **3.2.4 Formation pathways of C_{10} monomers without N-atoms and monomers with less than 10 C-atoms**

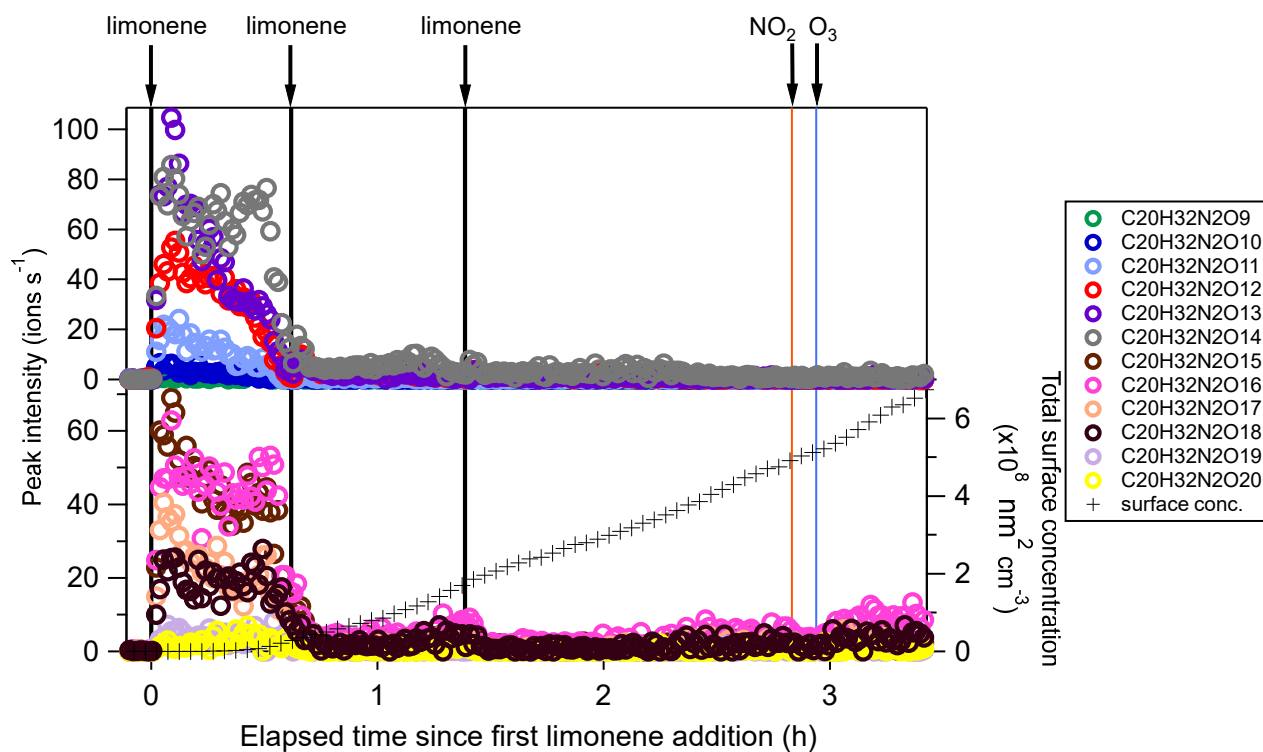
490 Besides C_{10} products containing nitrogen atoms, HOM monomers without nitrogen atoms were also identified.
491 Among these products, $\text{C}_{10}\text{H}_{14}\text{O}_x$ ($x=7-12$) were the most prevalent family, which were also detected in limonene
492 ozonolysis (Jokinen et al., 2015). The $\text{C}_{10}\text{H}_{14}\text{O}_x$ family showed a time series typical of first-generation products (Fig.
493 S8). $\text{C}_{10}\text{H}_{14}\text{O}_x$ and $\text{C}_{10}\text{H}_{16}\text{O}_x$ could be formed from limonene + NO_3 with $\text{C}_{10}\text{H}_{16}\text{NO}_x\bullet$ terminating their autoxidation
494 by migration of the $\alpha\text{-NO}_3$ H-atom, eliminating an NO_2 fragment (Scheme S2) (Novelli et al., 2021). Alternatively,
495 these products could be formed via the reaction of O_3 with limonene (Scheme S2). Either way, $\text{C}_{10}\text{H}_{14}\text{O}_x$ and
496 $\text{C}_{10}\text{H}_{16}\text{O}_x$ were formed via first-generation pathways.

497 We also observed monomers with carbon atom number less than 10. During the P1a period, C_9 monomer families
498 were the most abundant contributors to $\text{C}<10$ HOM monomers, followed by C_8 families. The majority of C_9
499 monomers were $\text{C}_9\text{H}_{15}\text{NO}_x$ ($x=7-13$) (time series shown in Fig. S9) and $\text{C}_9\text{H}_{13}\text{NO}_x$ ($x=8-14$). The loss of one carbon
500 atom may follow the mechanism shown in Scheme S3 (Fry et al., 2011; Bianchi et al., 2019). The major product
501 family in C_8 monomers is $\text{C}_8\text{H}_{11}\text{NO}_x$ ($x=6, 7, 9-13$). While during period P1a $\text{C}_8\text{H}_{11}\text{NO}_x$ compounds could be hardly
502 observed, their concentrations increased considerably in the later periods (Fig. S10). The gas-phase concentration of
503 $\text{C}_8\text{H}_{11}\text{NO}_7$ was even the highest among all compounds in later periods (highest intensity signal in Fig. 2b). This is
504 partly attributed to the relatively high volatility of C_8 compounds compared with C_{10} HOM species and accretion
505 products, which tend to condense on particles. The major family in C_7 monomers, $\text{C}_7\text{H}_9\text{NO}_x$ ($x=6-13$), showed a time
506 series pattern similar to $\text{C}_8\text{H}_{11}\text{NO}_x$ compounds (Fig. S11). Such a time profile indicates that C_7 and C_8 products were
507 likely a result of multi-generation gas-phase reactions.

508 **3.3 Dimers and their formation**

509 Among dimers, C_{20} products were the most abundant, followed by C_{19} products. Among C_{20} and C_{19} dimers, the most
510 prevalent families included $\text{C}_{20}\text{H}_{32}\text{N}_2\text{O}_x$ ($x=9-20$), $\text{C}_{20}\text{H}_{33}\text{N}_3\text{O}_x$ ($x=12-20$), $\text{C}_{20}\text{H}_{31}\text{NO}_x$ ($x=10-15$), $\text{C}_{20}\text{H}_{31}\text{N}_3\text{O}_x$
511 ($x=14-20$), $\text{C}_{20}\text{H}_{34}\text{N}_4\text{O}_x$ ($x=15-20$), and $\text{C}_{19}\text{H}_{30}\text{N}_2\text{O}_x$ ($x=10-18$) (Fig. S5). The O/C ratio of dimers did not exceed one,
512 while that of monomers was as high as two. This could be due to oxygen atom loss and participation of less
513 oxygenated $\text{RO}_2\bullet$ in the dimer formation as discussed below. Time series of dimers also showed different behavior
514 compared to monomers. For example, compounds of the $\text{C}_{20}\text{H}_{32}\text{N}_2\text{O}_x$ family only reached a considerable peak
515 intensity in period P1 and decreased rapidly thereafter, while the signal intensity in periods P2 to P6 were low (Fig.
516 5). Generally, other dimers showed similar patterns (Fig. S12-S14), though the difference of their concentration
517 between P2-P6 and P1 were not as large as for the $\text{C}_{20}\text{H}_{32}\text{N}_2\text{O}_x$ family. The time when signals of several dimers (e.g.
518 $\text{C}_{20}\text{H}_{32}\text{N}_2\text{O}_x$, $\text{C}_{20}\text{H}_{33}\text{N}_3\text{O}_x$, $\text{C}_{20}\text{H}_{34}\text{N}_4\text{O}_x$) dropped substantially matched the time of new particle formation (NPF) and
519 the onset of particle growth, indicating that some dimers were likely involved in the early growth of particles. Such

520 a behavior is expected since dimers have a much lower volatility than monomers. This observation is consistent with
 521 the limonene + NO₃ laboratory study by Faxon et al. (2018) that found a significant fraction of HOM dimer derived
 522 in the particle phase.
 523



524
 525 Figure 5. Time series of peak intensity of the C₂₀H₃₂N₂O_x family compounds during the periods P1 to P3. The cross
 526 markers (lower right y-axis) indicate total particle surface concentration.
 527

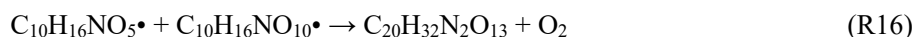
528 In general, C₂₀H₃₂N₂O_x showed an overlaying time profile of first- and second-generation products (Fig. 5).
 529 C₂₀H₃₂N₂O_x were likely formed via the accretion reaction between two monomer RO₂• (C₁₀H₁₆NO_x•):



531 Since C₁₀H₁₆NO_x• can be first- or second-generation products, the resulting dimers C₂₀H₃₂N₂O_x can also be first- or
 532 second-generation products. The time series show that C₂₀H₃₂N₂O_x with lower O number presented more of a first-
 533 generation product time profile (Fig. 5), while the relative contribution of second-generation formation was observed
 534 to increase with oxygen number.

535 We compared the observed dimer formula with those expected based on accretion reactions of HOM-RO₂•. X
 536 in the C₂₀H₃₂N₂O_x observed was ≥ 9; however, according to the accretion mechanism and the observed C₁₀H₁₆NO_x•
 537 (x ≥ 6), x in C₂₀H₃₂N₂O_x should be ≥ 10 (6+6-2=10). Moreover, as the most abundant RO₂• within the C₁₀H₁₆NO_x•
 538 family was C₁₀H₁₆NO₁₀• (Table 1), the most abundant C₂₀H₃₂N₂O_x would have an oxygen number of 18 if they were
 539 exclusively formed by the accretion reaction of HOM RO₂•. This contradicted the fact that the most abundant
 540 molecule among the C₂₀H₃₂N₂O_x family was C₂₀H₃₂N₂O₁₃. The findings above could only be explained by the

541 participation of less oxygenated RO₂• such as C₁₀H₁₆NO_{5,6}• in the accretion reaction (Berndt et al., 2018a; Berndt et
 542 al., 2018b; Mcfiggans et al., 2019). C₁₀H₁₆NO₅• was not detected by our CI-API-TOF, which is attributed to the lower
 543 detection sensitivity of molecules with O number ≤ 5 in the NO₃⁻-CIMS (Riva et al., 2019). Still, C₁₀H₁₆NO₅• is the
 544 first RO₂ radical formed in the limonene + NO₃ reaction (Scheme 1a) so a high mass flux has to pass through this
 545 RO₂•. If we assume that the abundance of C₁₀H₁₆NO₅• was high, and considering that the concentration of
 546 C₁₀H₁₆NO₁₀• was the highest in the C₁₀H₁₆NO_x• family, their accretion reaction (R16) could form C₂₀H₃₂N₂O₁₃ and
 547 support that C₂₀H₃₂N₂O₁₃ was the most abundant C₂₀ dimer product:



549 Time series of dimers with different numbers of N atoms were different, indicating different formation pathways.
 550 For example, the C₂₀H₃₁NO_x family were mainly first-generation products (Fig. S12), which may be formed via the
 551 following reaction:



553 C₁₀H₁₅O_x• were first-generation radicals (Sect. 3.2.4), while C₁₀H₁₆NO_x• were mainly second-generation radicals.
 554 C₁₀H₁₆NO_x• could also be formed via first-generation pathway as discussed above (Scheme 1a), but that was not
 555 borne out by the time profile, suggesting a fast termination of first-generation C₁₀H₁₆NO_x• radicals. Reaction R17
 556 could be one of the termination pathways of first-generation C₁₀H₁₆NO_x• based on the first-generation time profile
 557 of C₂₀H₃₁NO_x. In the study by Faxon et al. (2018), the formation of 1N-C₂₀ dimers was explained by a mechanism
 558 involving two 1N-RO₂ radicals which produced HNO₃ as a by-product. However, C₁₀ RO₂ radicals without nitrogen
 559 atoms were identified in our study, which provided a direct formation pathway of 1N-C₂₀ dimers through R17.

560 On the other hand, C₂₀H₃₃N₃O_x and C₂₀H₃₄N₄O_x were mainly second-generation products (Fig. S13, S14).
 561 C₂₀H₃₃N₃O_x and C₂₀H₃₄N₄O_x were likely to be formed via NO₃ oxidation of dimers containing less nitrogen atoms,
 562 and were thus second-generation products. The related radicals were also detected, such as C₂₀H₃₂N₃O_x• (x=16-19)
 563 and C₂₀H₃₁N₂O_x• (x=13-16). Possible formation pathways of dominant oligomer families are displayed in Table 2.
 564 We cannot exclude that the formation pathway of C₂₀H₃₃NO_x, C₂₀H₃₄N₄O_x and C₁₉H₃₁NO_x may also involve limonene
 565 oxidation by OH• (Table 2), which can be formed in the ozonolysis of limonene as a minor pathway. In addition, the
 566 high abundance of C₂₀H₃₁NO_x (x=10-15) among the dimers may be partly attributed to a contribution of the reaction
 567 of limonene with O₃.

568 The initial drop of the products (dimers and monomers) in Fig. 1, Fig. S8, and Fig. S12 during P1 (the
 569 characteristic time of the fastest decay was 15 min, 10 min, and 13 min, respectively) is attributed to the balance of
 570 their sources via the reaction of limonene with NO₃, their wall loss, and their potential loss by the reaction with NO₃.
 571 The characteristic time of the fastest decay of the HOM over the 2nd limonene addition in Fig. 1, 4, 5, S12, and S13
 572 are 4-8 min. These decays can be explained by the wall loss rate (characteristic time ~8 min) and condensation sink
 573 of vapor loss to particles according to the study of Kulmala et al. (2012) (characteristic time ~13 min). The
 574 characteristic times of the fastest decay of the HOM at the end of P2 in Fig. S12 and S13 are 1.4-3.4 min, which can
 575 also be well explained by the updated wall loss rate and condensation sink of vapor loss to particles at the end of P2

576 (characteristic time ~1.4 min).

577 In summary, HOM dimers are likely to be formed via accretion reactions of monomer RO_2^\bullet , and some dimers
578 can undergo secondary oxidation by NO_3 . Some dimers were likely involved in the early growth of SOA particles.

579

580

Table 2. Major dimer and trimer families and their possible formation pathways.

Dimer/Trimer family	Possible formation pathways
$\text{C}_{20}\text{H}_{32}\text{N}_2\text{O}_x$	$\text{C}_{10}\text{H}_{16}\text{NO}_x^\bullet + \text{C}_{10}\text{H}_{16}\text{NO}_x^\bullet$
$\text{C}_{20}\text{H}_{33}\text{N}_3\text{O}_x / \text{C}_{20}\text{H}_{31}\text{N}_3\text{O}_x$	$\text{C}_{20}\text{H}_{32}\text{N}_2\text{O}_x + \text{NO}_3 + \text{HO}_2^\bullet/\text{RO}_2^\bullet$
$\text{C}_{20}\text{H}_{31}\text{NO}_x$	$\text{C}_{10}\text{H}_{16}\text{NO}_x^\bullet + \text{C}_{10}\text{H}_{15}\text{O}_x^\bullet$
$\text{C}_{20}\text{H}_{33}\text{NO}_x$	$\text{C}_{10}\text{H}_{16} + \text{OH}^\bullet + \text{C}_{10}\text{H}_{16}\text{NO}_x^\bullet$
$\text{C}_{20}\text{H}_{34}\text{N}_4\text{O}_x$	$(\text{C}_{10}\text{H}_{16}\text{N}_2\text{O}_x + \text{OH}^\bullet) + (\text{C}_{10}\text{H}_{16}\text{N}_2\text{O}_x + \text{OH}^\bullet)$
$\text{C}_{19}\text{H}_{30}\text{N}_2\text{O}_x$	$\text{C}_{10}\text{H}_{16}\text{NO}_x^\bullet + \text{C}_9\text{H}_{14}\text{NO}_x^\bullet$
$\text{C}_{19}\text{H}_{31}\text{N}_3\text{O}_x$	$\text{C}_{19}\text{H}_{30}\text{N}_2\text{O}_x + \text{NO}_3 + \text{HO}_2^\bullet/\text{RO}_2^\bullet$
$\text{C}_{19}\text{H}_{29}\text{NO}_x$	$\text{C}_9\text{H}_{14}\text{NO}_x^\bullet + \text{C}_{10}\text{H}_{15}\text{O}_x^\bullet$
$\text{C}_{19}\text{H}_{31}\text{NO}_x$	$\text{C}_{10}\text{H}_{16} + \text{OH}^\bullet + \text{C}_9\text{H}_{14}\text{NO}_x^\bullet$
$\text{C}_{30}\text{H}_{48}\text{N}_4\text{O}_x$	$\text{C}_{20}\text{H}_{32}\text{N}_3\text{O}_x^\bullet + \text{C}_{10}\text{H}_{16}\text{NO}_x^\bullet$
$\text{C}_{30}\text{H}_{47}\text{N}_3\text{O}_x$	$\text{C}_{20}\text{H}_{31}\text{N}_2\text{O}_x^\bullet + \text{C}_{10}\text{H}_{16}\text{NO}_x^\bullet$

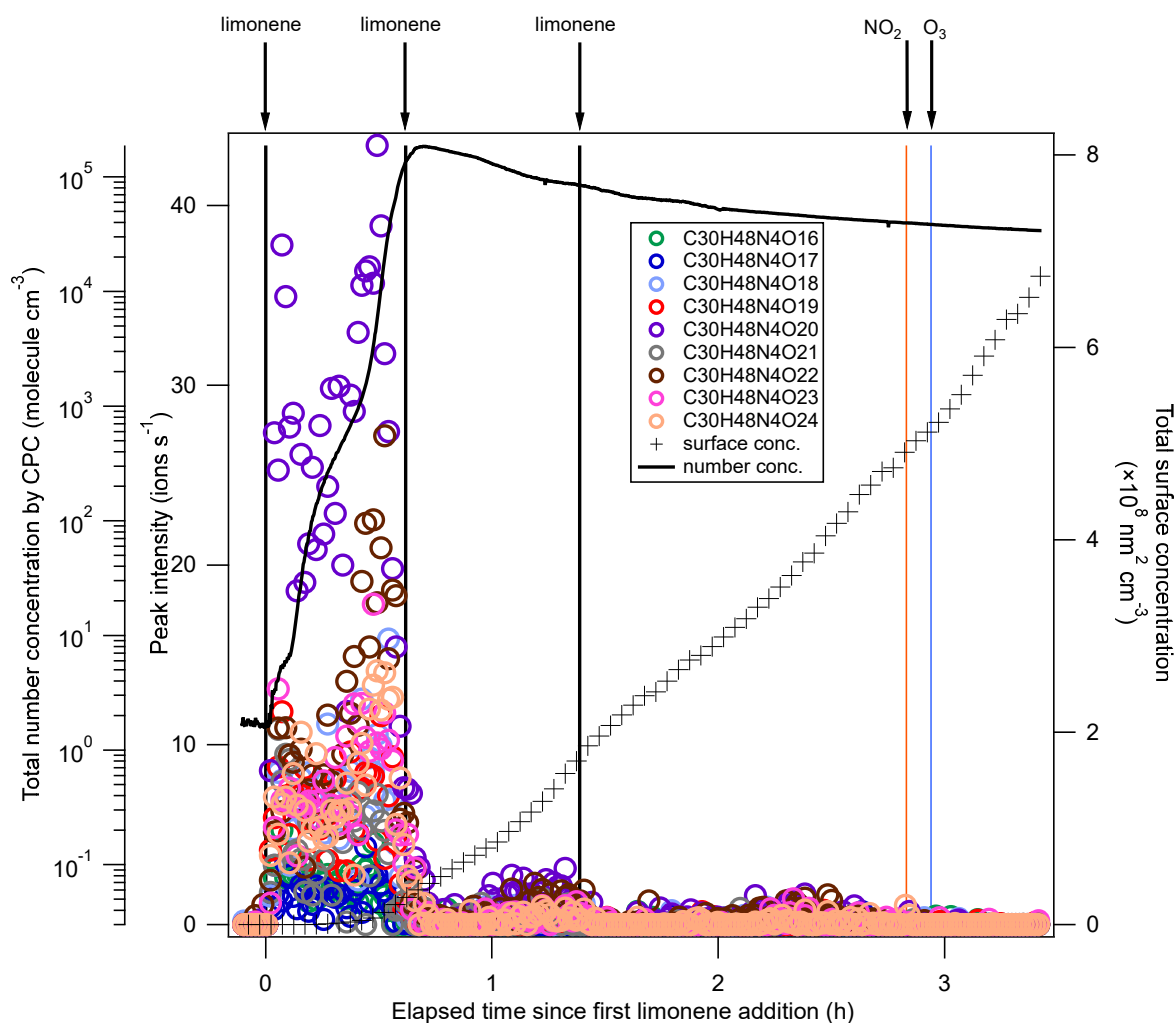
581

582 3.4 Trimers and their formation

583 Trimers (C_{26-30}) were dominated by C_{30} compounds (Fig. S6, Table S1). To the best of our knowledge, this is the first
584 study that identified gas-phase trimers in the limonene + NO_3 reaction. The O/C ratio of trimers were lower than that
585 of monomers and dimers, suggesting possible multiple accretion reactions in their formation pathways, which lose 2
586 oxygen atoms in each reaction. As each accretion reaction terminates the peroxy radical chain, the observation of
587 trimers also implies that some dimers could further react with NO_3 , creating dimer RO_2^\bullet . The most prevalent product
588 families were $\text{C}_{30}\text{H}_{48}\text{N}_4\text{O}_x$ ($x=16-24$) and $\text{C}_{30}\text{H}_{47}\text{N}_3\text{O}_x$ ($x=18,19,21,23,24$), which were likely formed via the most
589 abundant monomer RO_2 radicals - $\text{C}_{10}\text{H}_{16}\text{NO}_x^\bullet$ and the most abundant dimer RO_2 radicals - $\text{C}_{20}\text{H}_{32}\text{N}_3\text{O}_x^\bullet$ and
590 $\text{C}_{20}\text{H}_{31}\text{N}_2\text{O}_x^\bullet$. Trimers from other monoterpenes + NO_3 have been observed in previous laboratory studies. For
591 example, $\text{C}_{30}\text{H}_{48}\text{N}_4\text{O}_{16}$ and $\text{C}_{30}\text{H}_{47}\text{N}_3\text{O}_{16}$ were observed in the mass spectra of α -pinene + NO_3 SOA by Wu et al.
592 (2021a), and $\text{C}_{30}\text{H}_{47}\text{N}_3\text{O}_{13}$ was identified in β -pinene + NO_3 SOA by Claflin and Ziemann (2018).

593 Similar to their precursors $\text{C}_{20}\text{H}_{32}\text{N}_2\text{O}_x$, $\text{C}_{30}\text{H}_{48}\text{N}_4\text{O}_x$ showed negligible signal except in period P1, and presented
594 an overlaying time profile of first- and second-generation product pattern (Fig. 6). For comparison, gas-phase trimer
595 products were not observed in the β -pinene + NO_3 reaction (Shen et al., 2021), and the trimers observed in SOA from
596 β -pinene + NO_3 are likely formed via particle phase reactions (Claflin and Ziemann, 2018). An efficient gas-phase
597 trimer production via subsequent accretion reactions between peroxy radicals requires that the precursor dimer has a
598 high enough reactivity to create a dimer RO_2^\bullet , e.g. via NO_3 reaction to a double bond. This suggests that the VOC
599 containing at least two double bonds are likely more favorable to form trimers, which is consistent with our previous

600 findings that trimers were formed in the NO_3 reaction with isoprene which also contains two double bonds (Zhao et
 601 al., 2021) while they were not observed in the reaction of NO_3 with β -pinene which contains only one double bond
 602 (Shen et al., 2021).



603
 604 Figure 6. Time series of peak intensity of the $\text{C}_{30}\text{H}_{48}\text{N}_4\text{O}_x$ family compounds during the periods P1 to P3. The solid
 605 black line refers to total number concentrations detected by CPC. The cross markers (right y-axis) indicate total
 606 particle surface concentration.

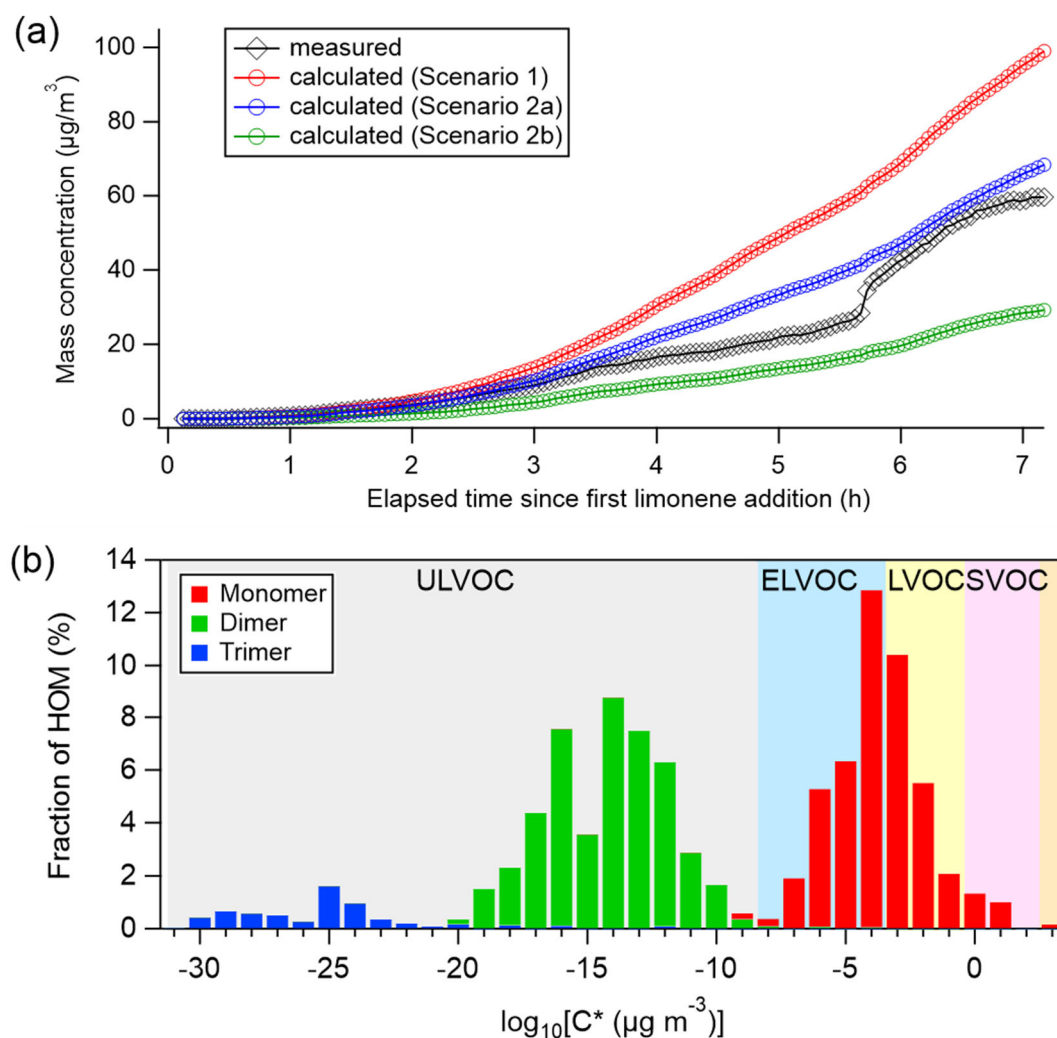
607
 608 **3.5 “Primary” incremental HOM yields**

609 We chose period P1 for the calculation of HOM yields in order to minimize the influence of the condensational sink
 610 on HOM concentration. However, both first-generation and second-generation products existed in this period, as
 611 discussed in Sect. 3.2 through 3.4 and supported by the time-behavior of the total HOM concentration (Fig. S15).
 612 Period P1 can be roughly divided into three phases based on the trends in HOM concentration. Shortly after the
 613 limonene injection, large quantities of HOM were produced (first-production phase) followed by a balanced
 614 intermediate phase when HOM concentrations stopped increasing. After the intermediate phase, HOM concentrations
 615 began to increase again (second-production phase). The first-production phase overlapped with the time span where

616 limonene, NO_3 and N_2O_5 concentrations decreased, implying the dominance of first-generation HOM production
 617 process. During the second production period, wall loss was compensated by second-generation HOM formation,
 618 leading to another rise of the total HOM concentrations. Therefore, we use the first-production phase to estimate
 619 primary HOM production, determined over the first 3 min of the experiment. The calculated “primary” HOM molar
 620 yield is $1.5\%_{-0.7\%}^{+1.7\%}$. This value is significantly lower than the HOM yield of 5 to 17 % in earlier limonene ozonolysis
 621 experiments (Ehn et al., 2014; Jokinen et al., 2015; Pagonis et al., 2019). It should be emphasized that second-
 622 generation HOM, which contributed greatly to the limonene + NO_3 reaction system, is not included in this primary
 623 HOM yield.

624

625 3.6 Contribution of HOM to particle formation and growth



626

627 Figure 7. (a) Comparison of measured particle concentrations (black) against those predicted from condensation of
 628 measured HOM on aerosol particles, where red markers were calculated under Scenario 1, blue and green markers
 629 were calculated under Scenario 2 (only considering the condensation of ULVOC, ELVOC and LVOC), with the
 630 volatility calculated using the method by Mohr et al. (2019) (Scenario 2a) and Peräkylä et al. (2020) (Scenario 2b)

631 respectively. (b) HOM volatility distribution using formula provided by Mohr et al. (2019). Average concentrations
632 of HOM in the P1 period were used to calculate the fraction of HOM.

633

634 We observed nucleation and growth of SOA particles in the limonene + NO₃ reaction. We calculated the contribution
635 of HOM to SOA formation and particle growth and compared it to the measured particle growth (Fig. 7a). We
636 assumed different scenarios of HOM uptake on aerosol particles, using the calculation methods described in the
637 literature (Ehn et al., 2014; Seinfeld and Pandis, 2006; Nieminen et al., 2010). The assumption that all HOM
638 irreversibly condense on the particles (Scenario 1) resulted in a strong overestimation of particle mass growth (red
639 markers in Fig. 7a). Applying the parameterizations of Mohr et al. (2019) (Scenario 2a) or Peräkylä et al. (2020)
640 (Scenario 2b) for classification and accounting only LVOC- and ULVOC/ELVOC-HOM for irreversible uptake
641 framed the observed values (blue and green markers in Fig. 7a). While Scenario 2a agreed quite well with the
642 observations and only slightly overestimated SOA concentrations after 7 h by +11%, Scenario 2b underestimated the
643 SOA concentration at the end by -53%. The agreement between the modeled and observed SOA concentration
644 suggests that HOM, and particularly LVOC- and ULVOC/ELVOC-HOM play a major role in growth of SOA particles
645 in this study. This is consistent with the work by Faxon et al. (2018) who found that many of the dimers are ELVOC,
646 which is also supported by our calculation result based on the method of Mohr et al. (2019).

647 Since neither SO₂ nor H₂SO₄ was added in our experiment, new particle formation (NPF) could be attributed to
648 the nucleation initiated by HOM of low volatility. HOM trimers with as many as 30 carbon atoms were identified in
649 the early stage of this study, and their sudden loss matched the onset of rapid formation of SOA. Trimers identified
650 in our experiment are classified as ULVOC/ELVOC, with much lower volatility than monomers and dimers (Fig. 7b).
651 Therefore, NPF in the current study can more likely be attributed to HOM trimers since they have the strongest
652 potential of initiating nucleation, although we cannot rule out some contributions of dimers in the NPF. In contrast,
653 in an earlier experiment investigating the NO₃-initiated oxidation of β-pinene also conducted in the SAPHIR chamber
654 under similar conditions, new particles were barely formed (<20 cm⁻³) (Shen et al., 2021). As already mentioned
655 above, no trimer HOM products were observed in that study, and only molecules with C_≤20 were detected (Sect. 3.4).
656 Extremely low volatile organic vapors formed in α-pinene ozonolysis have been shown to induce nucleation and
657 drive initial particle growth in the atmosphere (Tröstl et al., 2016; Kirkby et al., 2016). Since our experiment of NO₃
658 oxidation of limonene was performed under near atmospheric conditions, such NPF events induced by the oxidation
659 of limonene by NO₃ could also occur in the ambient atmosphere. Although monoterpene concentrations in this study
660 (0-0.92 ppbv) are higher than in most ambient regions, they are still in the range of ambient concentrations (~0.01-1
661 ppbv) (e.g. Coggon et al., 2021; Wang et al., 2022), especially for forested regions (e.g. Xu et al., 2015; Kontkanen
662 et al., 2016; Janson, 1992). Assuming that dimers react with NO₃ at a rate similar to limonene, and that they have a
663 condensation sink similar to H₂SO₄ (10⁻³-10⁻¹ s⁻¹) (Dada et al., 2020), the lifetime with respect to NO₃ at an NO₃
664 concentration of 5-300 ppt and to condensation on particles are ~0.1-10 min and ~0.1-20 min, respectively. Therefore,
665 although aerosols may scavenge HOM dimers in the ambient atmosphere, dimers can still react with NO₃ at nighttime,

666 forming trimers. Such reactions are particularly important when the ambient aerosol concentration is low. Several
667 field observations have shown NPF events taking place at nighttime where biogenic emissions dominate (Kammer
668 et al., 2018; Huang et al., 2019). The work by Ortega et al. (2012) demonstrated an important role of monoterpene
669 ozonolysis products in nocturnal NPF events in chamber experiments. In a previous laboratory study, limonene +
670 NO₃ appears more effective at initiating nucleation than the limonene + O₃ reaction (Fry et al., 2014), which supports
671 that limonene + NO₃ can play a significant role in nighttime nucleation. Our study suggests that NO₃ oxidation of
672 limonene could contribute to the nighttime NPF via HOM trimer formation. In contrast, we infer that NO₃ reactions
673 with other monoterpenes containing only one double bond such as α -pinene and β -pinene are less likely candidates
674 for nighttime NPF, because gas-phase trimers are not observed.

675

676 **4 Conclusion and implications**

677 HOM formation in the reaction of limonene with NO₃ was investigated in the SAPHIR chamber. About 280 gas-
678 phase HOM products were identified, including monomers (C₆₋₁₀, O₆₋₁₆, N₀₋₃), dimers (C₁₇₋₂₀, O₇₋₂₀, N₀₋₄) and trimers
679 (C₂₇₋₃₀, O₁₆₋₂₅, N₁₋₆). Nitrogen-containing products dominated the HOM, with compounds of the C₁₀H₁₅₋₁₇NO₆₋₁₄
680 series being the most prevalent. Dimers contributed 47 % in the early stage of the experiment when particle surface
681 concentration was rather low ($< 6 \times 10^4 \text{ nm}^2 \text{ cm}^{-3}$), which was similar to monomers (47 %). Tentative formation
682 pathways of major families were proposed in this work based on their time-dependent concentration profiles.

683 In HOM monomers, the abundance of carbonyl compounds significantly exceeded that of hydroxy or
684 hydroperoxy compounds, indicating the significance of unimolecular termination of HOM-RO₂ radicals. Both RO₂•
685 autoxidation and alkoxy-peroxy pathways were found to be important in the formation of HOM monomers.
686 Monomers with 1 nitrogen atom (1N-monomers) contained both first- and second-generation products, which could
687 be formed via NO₃ oxidation of limonene and its first-generation products with the latter being more important.
688 Monomers with 2 nitrogen atoms were classified as second-generation products, which could be formed via NO₃
689 oxidation of the remaining C=C double bond of 1N-monomers.

690 Dimers showed both first- and second-generation time pattern. Dimers were mostly formed via accretion
691 reactions between monomer RO₂ radicals, resulting in a decrease in O/C ratio compared to monomers. The initial
692 less oxygenated RO₂•, including the C₁₀H₁₆NO₅• radical that cannot be observed in our instrument, likely played an
693 important role in dimer formation based on the comparison of measured dimers against expected dimer identity and
694 concentrations according to accretion monomer RO₂• reactions. Trimers were likely formed via accretion reactions
695 between monomer RO₂ and dimer RO₂ radicals formed from secondary reactions of dimers with NO₃. Trimer
696 formation is thus linked to the presence of two double bonds in limonene, of which the first reacts with NO₃ leading
697 to dimer products while the remaining C=C double bond provides a reactive site for further oxidation of the dimers
698 by NO₃, forming dimer RO₂ radicals.

699 A “primary” HOM molar yield of $1.5 \%_{\pm 0.7}^{+1.7\%}$ in the limonene + NO₃ reaction was estimated, including only the
700 first-generation HOM. Second-generation HOM contributed greatly to monomers, dimers and trimers, and hence the

701 HOM yield we obtained is a lower limit of the total HOM yield, and is likewise much lower than the total HOM yield
702 in the reaction of limonene with ozone (5 to 17 %) (Ehn et al., 2014; Jokinen et al., 2015; Pagonis et al., 2019).

703 NPF observed in this work was likely related to the trimer formation due to much lower volatility of trimers
704 compared to monomers and dimers. The SOA concentration in the limonene + NO₃ reaction could be explained by
705 the condensation of the HOM belonging to LVOC and ULVOC/ELVOC classes assuming irreversible uptake,
706 indicating an important role of HOM for growth of SOA particles in this reaction system. To our knowledge, this
707 work is the first identifying trimer products from the limonene + NO₃ reaction system, suggesting that limonene +
708 NO₃ is a possible crucial source of new particles formed in nighttime biogenic emission-dominated areas (Kammer
709 et al., 2018; Huang et al., 2019). Our work highlights the need to consider the role of limonene + NO₃ in NPF in
710 models simulating nighttime aerosols formation in biogenic-emission dominated areas, especially with large
711 limonene emissions. In addition, comparison with the reactions of NO₃ with isoprene (Zhao et al., 2021) and other
712 monoterpenes (Shen et al., 2021) reveals a strong dependence of HOM products on the molecular structure of the
713 VOC species in NO₃-initiated chemistry.

714 The concentration of limonene and NO₃ in this study were on the order of few ppb and a few to one hundred
715 ppt, respectively, which are similar to the ambient levels in rural and forest regions affected by anthropogenic
716 emissions (Brown and Stutz, 2012). The chemical lifetime of RO₂• was of the order of 50 to 500 s, which is also
717 similar to ambient conditions at nighttime (Fry et al., 2018). The RO₂• loss pathway in our study was dominated by
718 the reactions RO₂• + NO₃ and RO₂• + RO₂•, which is relevant for the RO₂• fate in urban areas and forested areas
719 influenced by an urban plume at nighttime. However, in more pristine forested regions, the RO₂• fate is mostly
720 determined by RO₂• + HO₂ and RO₂• + RO₂•, as shown by Bates et al. (2022) for the example of a Southeast US
721 forest. As NO₃ concentration is generally enhanced with increased anthropogenic emissions, RO₂• + NO₃ will become
722 more important going from remote to urban areas. Therefore, the HOM products and their formation process in our
723 study are relevant for rural and forested regions influenced by anthropogenic plumes and ambient urban regions with
724 high volatile commercial products emissions as limonene is a typical component of volatile chemical products (VCP)
725 (Nazaroff and Weschler, 2004). In these regions, HOM from monoterpene + NO₃ reactions can be major components
726 of nighttime SOA. As nitrooxy-RO₂ fate can strongly affect the oxidation product distribution and SOA yield as
727 shown for the reaction of α -pinene with NO₃ (Bates et al., 2022), more studies of HOM formation by NO₃ at various
728 RO₂• fates are needed to be representative of various environment including (remote) forested regions.

729 This study also highlights the important role of second-generation chemistry in HOM formation, which needs
730 to be further investigated and should be included in chemical mechanism used in numerical models. Additional work
731 is also needed to investigate the role of different HOM formed via NO₃-initiated BVOC oxidation reactions in NPF
732 and growth of SOA particles in order to better constrain the climatic and environmental effects of BVOC + NO₃
733 chemistry.

734

735 Acknowledgement

736 Y. Guo, H. Shen, H. Luo, and D. Zhao would like to thank the funding support of Science and Technology
737 Commission of Shanghai Municipality (No. 20230711400), National Natural Science Foundation of China (No.
738 41875145), and Shanghai International Science and Technology Partnership Project (No. 21230780200). Sungah
739 Kang, Astrid Kiendler-Scharr, and Thomas F. Mentel acknowledge the support by the EU Project FORCeS (grant
740 agreement no. 821205).

741 **References**

- 742 Ayres, B. R., Allen, H. M., Draper, D. C., Brown, S. S., Wild, R. J., Jimenez, J. L., Day, D. A., Campuzano-Jost, P., Hu, W.,
743 de Gouw, J., Koss, A., Cohen, R. C., Duffey, K. C., Romer, P., Baumann, K., Edgerton, E., Takahama, S., Thornton,
744 J. A., Lee, B. H., Lopez-Hilfiker, F. D., Mohr, C., Wennberg, P. O., Nguyen, T. B., Teng, A., Goldstein, A. H.,
745 Olson, K., and Fry, J. L.: Organic nitrate aerosol formation via NO_3 + biogenic volatile organic compounds in the
746 southeastern United States, *Atmos. Chem. Phys.*, 15, 13377-13392, 10.5194/acp-15-13377-2015, 2015.
- 747 Bates, K. H., Burke, G. J. P., Cope, J. D., and Nguyen, T. B.: Secondary organic aerosol and organic nitrogen yields from
748 the nitrate radical (NO_3) oxidation of alpha-pinene from various RO_2 fates, *Atmos. Chem. Phys.*, 22, 1467-1482,
749 10.5194/acp-22-1467-2022, 2022.
- 750 Beaver, M. R., Clair, J. M. S., Paulot, F., Spencer, K. M., Crouse, J. D., LaFranchi, B. W., Min, K. E., Pusede, S. E.,
751 Wooldridge, P. J., Schade, G. W., Park, C., Cohen, R. C., and Wennberg, P. O.: Importance of biogenic precursors
752 to the budget of organic nitrates: observations of multifunctional organic nitrates by CIMS and TD-LIF during
753 BEARPEX 2009, *Atmos. Chem. Phys.*, 12, 5773-5785, 10.5194/acp-12-5773-2012, 2012.
- 754 Bell, D. M., Wu, C., Bertrand, A., Graham, E., Schoonbaert, J., Giannoukos, S., Baltensperger, U., Prevot, A. S. H., Riipinen,
755 I., El Haddad, I., and Mohr, C.: Particle-phase processing of α -pinene NO_3 secondary organic aerosol in the dark,
756 *Atmos. Chem. Phys. Discuss.*, 2021, 1-28, 10.5194/acp-2021-379, 2021.
- 757 Berkemeier, T., Takeuchi, M., Eris, G., and Ng, N. L.: Kinetic modeling of formation and evaporation of secondary organic
758 aerosol from NO_3 oxidation of pure and mixed monoterpenes, *Atmos. Chem. Phys.*, 20, 15513-15535,
759 10.5194/acp-20-15513-2020, 2020.
- 760 Berndt, T., Mender, B., Scholz, W., Fischer, L., Herrmann, H., Kulmala, M., and Hansel, A.: Accretion Product Formation
761 from Ozonolysis and OH Radical Reaction of α -Pinene: Mechanistic Insight and the Influence of Isoprene and
762 Ethylene, *Environ. Sci. Technol.*, 52, 11069-11077, 10.1021/acs.est.8b02210, 2018a.
- 763 Berndt, T., Scholz, W., Mentler, B., Fischer, L., Herrmann, H., Kulmala, M., and Hansel, A.: Accretion Product Formation
764 from Self- and Cross-Reactions of RO_2 Radicals in the Atmosphere, *Angew. Chem. Int. Edit.*, 57, 3820-3824,
765 10.1002/anie.201710989, 2018b.
- 766 Bianchi, F., Kurtén, T., Riva, M., Mohr, C., Rissanen, M. P., Roldin, P., Berndt, T., Crouse, J. D., Wennberg, P. O., Mentel,
767 T. F., Wildt, J., Junninen, H., Jokinen, T., Kulmala, M., Worsnop, D. R., Thornton, J. A., Donahue, N., Kjaergaard,
768 H. G., and Ehn, M.: Highly Oxygenated Organic Molecules (HOM) from Gas-Phase Autoxidation Involving
769 Peroxy Radicals: A Key Contributor to Atmospheric Aerosol, *Chem. Rev.*, 119, 3472-3509,
770 10.1021/acs.chemrev.8b00395, 2019.
- 771 Boyd, C. M., Nah, T., Xu, L., Berkemeier, T., and Ng, N. L.: Secondary Organic Aerosol (SOA) from Nitrate Radical
772 Oxidation of Monoterpenes: Effects of Temperature, Dilution, and Humidity on Aerosol Formation, Mixing, and
773 Evaporation, *Environ. Sci. Technol.*, 51, 7831-7841, 10.1021/acs.est.7b01460, 2017.
- 774 Boyd, C. M., Sanchez, J., Xu, L., Eugene, A. J., Nah, T., Tuet, W. Y., Guzman, M. I., and Ng, N. L.: Secondary organic
775 aerosol formation from the β -pinene+ NO_3 system: effect of humidity and peroxy radical fate, *Atmos. Chem. Phys.*,
776 15, 7497-7522, 10.5194/acp-15-7497-2015, 2015.
- 777 Brown, S. S. and Stutz, J.: Nighttime radical observations and chemistry, *Chem. Soc. Rev.*, 41, 6405-6447,
778 10.1039/c2cs35181a, 2012.
- 779 Carslaw, N., Mota, T., Jenkin, M. E., Barley, M. H., and McFiggans, G.: A significant role for nitrate and peroxide groups
780 on indoor secondary organic aerosol, *Environ. Sci. Technol.*, 46, 9290-9298, 10.1021/es301350x, 2012.
- 781 Chen, Y., Takeuchi, M., Nah, T., Xu, L., Canagaratna, M. R., Stark, H., Baumann, K., Canonaco, F., Prévôt, A. S. H., Huey,
782 L. G., Weber, R. J., and Ng, N. L.: Chemical characterization of secondary organic aerosol at a rural site in the
783 southeastern US: insights from simultaneous high-resolution time-of-flight aerosol mass spectrometer (HR-ToF-
784 AMS) and FIGAERO chemical ionization mass spectrometer (CIMS) measurements, *Atmos. Chem. Phys.*, 20,

785 8421-8440, 10.5194/acp-20-8421-2020, 2020.

786 Claflin, M. S. and Ziemann, P. J.: Identification and Quantitation of Aerosol Products of the Reaction of β -Pinene with NO_3
787 Radicals and Implications for Gas- and Particle-Phase Reaction Mechanisms, *J. Phys. Chem. A*, 122, 3640-3652,
788 10.1021/acs.jpca.8b00692, 2018.

789 Clausen, P. A., Wilkins, C. K., Wolkoff, P., and Nielsen, G. D.: Chemical and biological evaluation of a reaction mixture
790 of R-(+)-limonene/ozone - Formation of strong airway irritants, *Environ. Int.*, 26, 511-522, 10.1016/s0160-
791 4120(01)00035-6, 2001.

792 Coggon, M. M., Gkatzelis, G. I., McDonald, B. C., Gilman, J. B., Schwantes, R. H., Abuhassan, N., Aikin, K. C., Arend,
793 M. F., Berkoff, T. A., Brown, S. S., Campos, T. L., Dickerson, R. R., Gronoff, G., Hurley, J. F., Isaacman-VanWertz,
794 G., Koss, A. R., Li, M., McKeen, S. A., Moshary, F., Peischl, J., Pospisilova, V., Ren, X., Wilson, A., Wu, Y.,
795 Trainer, M., and Warneke, C.: Volatile chemical product emissions enhance ozone and modulate urban chemistry,
796 *Proc. Nat. Acad. Sci. U.S.A.*, 118, 10.1073/pnas.2026653118, 2021.

797 Crounse, J. D., Nielsen, L. B., Jørgensen, S., Kjaergaard, H. G., and Wennberg, P. O.: Autoxidation of Organic Compounds
798 in the Atmosphere, *J. Phys. Chem. Lett.*, 4, 3513-3520, 10.1021/jz4019207, 2013.

799 Dada, L., Ylivinkka, I., Baalbaki, R., Li, C., Guo, Y., Yan, C., Yao, L., Sarnela, N., Jokinen, T., Daellenbach, K. R., Yin, R.,
800 Deng, C., Chu, B., Nieminen, T., Wang, Y., Lin, Z., Thakur, R. C., Kontkanen, J., Stolzenburg, D., Sipilä, M.,
801 Hussein, T., Paasonen, P., Bianchi, F., Salma, I., Weidinger, T., Pikridas, M., Sciare, J., Jiang, J., Liu, Y., Petäjä,
802 T., Kerminen, V.-M., and Kulmala, M.: Sources and sinks driving sulfuric acid concentrations in contrasting
803 environments: implications on proxy calculations, *Atmos. Chem. Phys.*, 20, 11747-11766, 10.5194/acp-20-11747-
804 2020, 2020.

805 Dam, M., Draper, D. C., Marsavin, A., Fry, J. L., and Smith, J. N.: Observations of gas-phase products from the nitrate-
806 radical-initiated oxidation of four monoterpenes, *Atmos. Chem. Phys.*, 22, 9017-9031, 10.5194/acp-22-9017-2022,
807 2022.

808 Donahue, N. M., Epstein, S. A., Pandis, S. N., and Robinson, A. L.: A two-dimensional volatility basis set: 1. organic-
809 aerosol mixing thermodynamics, *Atmos. Chem. Phys.*, 11, 3303-3318, 10.5194/acp-11-3303-2011, 2011.

810 Donahue, N. M., Kroll, J. H., Pandis, S. N., and Robinson, A. L.: A two-dimensional volatility basis set – Part 2: Diagnostics
811 of organic-aerosol evolution, *Atmos. Chem. Phys.*, 12, 615-634, 10.5194/acp-12-615-2012, 2012.

812 Ehn, M., Thornton, J. A., Kleist, E., Sipilä, M., Junninen, H., Pullinen, I., Springer, M., Rubach, F., Tillmann, R., Lee, B.,
813 Lopez-Hilfiker, F., Andres, S., Acir, I. H., Rissanen, M., Jokinen, T., Schobesberger, S., Kangasluoma, J.,
814 Kontkanen, J., Nieminen, T., Kurtén, T., Nielsen, L. B., Jørgensen, S., Kjaergaard, H. G., Canagaratna, M., Dal
815 Maso, M., Berndt, T., Petäjä, T., Wahner, A., Kerminen, V. M., Kulmala, M., Worsnop, D. R., Wildt, J., and Mentel,
816 T. F.: A large source of low-volatility secondary organic aerosol, *Nature*, 506, 476-485, 10.1038/nature13032,
817 2014.

818 Eisele, F. L. and Tanner, D. J.: Measurement of the gas phase concentration of H_2SO_4 and methane sulfonic acid and
819 estimates of H_2SO_4 production and loss in the atmosphere, *J. Geophys. Res.-Atmos.*, 98, 9001-9010,
820 10.1029/93jd00031, 1993.

821 Fan, Z. H., Liou, P., Weschler, C., Fiedler, N., Kipen, H., and Zhang, J. F.: Ozone-initiated reactions with mixtures of
822 volatile organic compounds under simulated indoor conditions, *Environ. Sci. Technol.*, 37, 1811-1821,
823 10.1021/es026231i, 2003.

824 Faxon, C., Hammes, J., Le Breton, M., Pathak, R. K., and Hallquist, M.: Characterization of organic nitrate constituents of
825 secondary organic aerosol (SOA) from nitrate-radical-initiated oxidation of limonene using high-resolution
826 chemical ionization mass spectrometry, *Atmos. Chem. Phys.*, 18, 5467-5481, 10.5194/acp-18-5467-2018, 2018.

827 Finlayson-Pitts, B. J. and Pitts, J. N.: Tropospheric air pollution: Ozone, airborne toxics, polycyclic aromatic hydrocarbons,
828 and particles, *Science*, 276, 1045-1052, 10.1126/science.276.5315.1045, 1997.

829 Fry, J. L., Draper, D. C., Barsanti, K. C., Smith, J. N., Ortega, J., Winkler, P. M., Lawler, M. J., Brown, S. S., Edwards, P.
830 M., Cohen, R. C., and Lee, L.: Secondary organic aerosol formation and organic nitrate yield from NO₃ oxidation
831 of biogenic hydrocarbons, *Environ. Sci. Technol.*, 48, 11944-11953, 10.1021/es502204x, 2014.

832 Fry, J. L., Kiendler-Scharr, A., Rollins, A. W., Wooldridge, P. J., Brown, S. S., Fuchs, H., Dubé, W., Mensah, A., dal Maso,
833 M., Tillmann, R., Dorn, H. P., Brauers, T., and Cohen, R. C.: Organic nitrate and secondary organic aerosol yield
834 from NO₃ oxidation of β-pinene evaluated using a gas-phase kinetics/aerosol partitioning model, *Atmos. Chem.
835 Phys.*, 9, 1431-1449, 10.5194/acp-9-1431-2009, 2009.

836 Fry, J. L., Kiendler-Scharr, A., Rollins, A. W., Brauers, T., Brown, S. S., Dorn, H. P., Dubé, W. P., Fuchs, H., Mensah, A.,
837 Rohrer, F., Tillmann, R., Wahner, A., Wooldridge, P. J., and Cohen, R. C.: SOA from limonene: role of NO₃ in its
838 generation and degradation, *Atmos. Chem. Phys.*, 11, 3879-3894, 10.5194/acp-11-3879-2011, 2011.

839 Fry, J. L., Draper, D. C., Zorzana, K. J., Campuzano-Jost, P., Day, D. A., Jimenez, J. L., Brown, S. S., Cohen, R. C., Kaser,
840 L., Hansel, A., Cappellin, L., Karl, T., Hodzic Roux, A., Turnipseed, A., Cantrell, C., Lefer, B. L., and Grossberg,
841 N.: Observations of gas- and aerosol-phase organic nitrates at BEACHON-RoMBAS 2011, *Atmos. Chem. Phys.*,
842 13, 8585-8605, 10.5194/acp-13-8585-2013, 2013.

843 Fry, J. L., Brown, S. S., Middlebrook, A. M., Edwards, P. M., Campuzano-Jost, P., Day, D. A., Jimenez, J. L., Allen, H. M.,
844 Ryerson, T. B., Pollack, I., Graus, M., Warneke, C., de Gouw, J. A., Brock, C. A., Gilman, J., Lerner, B. M., Dubé,
845 W. P., Liao, J., and Welti, A.: Secondary organic aerosol (SOA) yields from NO₃ radical + isoprene based on
846 nighttime aircraft power plant plume transects, *Atmos. Chem. Phys.*, 18, 11663-11682, 10.5194/acp-18-11663-
847 2018, 2018.

848 Fuchs, H., Hofzumahaus, A., Rohrer, F., Bohn, B., Brauers, T., Dorn, H. P., Häsel, R., Holland, F., Kaminski, M., Li, X.,
849 Lu, K., Nehr, S., Tillmann, R., Wegener, R., and Wahner, A.: Experimental evidence for efficient hydroxyl radical
850 regeneration in isoprene oxidation, *Nat. Geosci.*, 6, 1023-1026, 10.1038/ngeo1964, 2013.

851 Fuchs, N. A. and Sutugin, A. G.: *Topics in Current Aerosol Research (Part 2)*, Pergamon, New York, 1971.

852 Gkatzelis, G. I., Coggon, M. M., McDonald, B. C., Peischl, J., Aikin, K. C., Gilman, J. B., Trainer, M., and Warneke, C.:
853 Identifying Volatile Chemical Product Tracer Compounds in U.S. Cities, *Environ. Sci. Technol.*, 55, 188-199,
854 10.1021/acs.est.0c05467, 2021.

855 Guenther, A. B., Jiang, X., Heald, C. L., Sakulyanontvittaya, T., Duhl, T., Emmons, L. K., and Wang, X.: The Model of
856 Emissions of Gases and Aerosols from Nature version 2.1 (MEGAN2.1): an extended and updated framework for
857 modeling biogenic emissions, *Geosci. Model Dev.*, 5, 1471-1492, 10.5194/gmd-5-1471-2012, 2012.

858 Hallquist, M., Wängberg, I., Ljungström, E., Barnes, I., and Becker, K. H.: Aerosol and product yields from NO₃ radical-
859 initiated oxidation of selected monoterpenes, *Environ. Sci. Technol.*, 33, 553-559, 10.1021/es980292s, 1999.

860 Hallquist, M., Wenger, J. C., Baltensperger, U., Rudich, Y., Simpson, D., Claeys, M., Dommen, J., Donahue, N. M., George,
861 C., Goldstein, A. H., Hamilton, J. F., Herrmann, H., Hoffmann, T., Iinuma, Y., Jang, M., Jenkin, M. E., Jimenez,
862 J. L., Kiendler-Scharr, A., Maenhaut, W., McFiggans, G., Mentel, T. F., Monod, A., Prévôt, A. S. H., Seinfeld, J.
863 H., Surratt, J. D., Szmigielski, R., and Wildt, J.: The formation, properties and impact of secondary organic aerosol:
864 current and emerging issues, *Atmos. Chem. Phys.*, 9, 5155-5236, 10.5194/acp-9-5155-2009, 2009.

865 Huang, W., Saathoff, H., Shen, X., Ramisetty, R., Leisner, T., and Mohr, C.: Chemical Characterization of Highly
866 Functionalized Organonitrates Contributing to Night-Time Organic Aerosol Mass Loadings and Particle Growth,
867 *Environ. Sci. Technol.*, 53, 1165-1174, 10.1021/acs.est.8b05826, 2019.

868 Hyttinen, N., Kupiainen-Määttä, O., Rissanen, M. P., Muuronen, M., Ehn, M., and Kurtén, T.: Modeling the Charging of
869 Highly Oxidized Cyclohexene Ozonolysis Products Using Nitrate-Based Chemical Ionization, *J. Phys. Chem. A*,
870 119, 6339-6345, 10.1021/acs.jpca.5b01818, 2015.

871 Janson, R.: Monoterpene concentrations in and above a forest of scots pine, *J. Atmos. Chem.*, 14, 385-394,
872 10.1007/bf00115246, 1992.

873 Jenkin, M. E., Saunders, S. M., and Pilling, M. J.: The tropospheric degradation of volatile organic compounds: A protocol
874 for mechanism development, *Atmos. Environ.*, 31, 81-104, 10.1016/s1352-2310(96)00105-7, 1997.

875 Jiang, L., Wang, W., and Xu, Y. S.: Theoretical investigation of the NO₃ radical addition to double bonds of limonene, *Int.*
876 *J. Mol. Sci.*, 10, 3743-3754, 10.3390/ijms10093743, 2009.

877 Jokinen, T., Sipilä, M., Junninen, H., Ehn, M., Lönn, G., Hakala, J., Petäjä, T., Mauldin, R. L., Kulmala, M., and Worsnop,
878 D. R.: Atmospheric sulphuric acid and neutral cluster measurements using CI-API-TOF, *Atmos. Chem. Phys.*, 12,
879 4117-4125, 10.5194/acp-12-4117-2012, 2012.

880 Jokinen, T., Berndt, T., Makkonen, R., Kerminen, V. M., Junninen, H., Paasonen, P., Stratmann, F., Herrmann, H., Guenther,
881 A. B., Worsnop, D. R., Kulmala, M., Ehn, M., and Sipilä, M.: Production of extremely low volatile organic
882 compounds from biogenic emissions: Measured yields and atmospheric implications, *P. Natl. Acad. Sci. USA*,
883 112, 7123-7128, 10.1073/pnas.1423977112, 2015.

884 Kammer, J., Perraudin, E., Flaud, P. M., Lamaud, E., Bonnefond, J. M., and Villenave, E.: Observation of nighttime new
885 particle formation over the French Landes forest, *Sci. Total Environ.*, 621, 1084-1092,
886 10.1016/j.scitotenv.2017.10.118, 2018.

887 Kirkby, J., Duplissy, J., Sengupta, K., Frege, C., Gordon, H., Williamson, C., Heinritzi, M., Simon, M., Yan, C., Almeida,
888 J., Tröstl, J., Nieminen, T., Ortega, I. K., Wagner, R., Adamov, A., Amorim, A., Bernhammer, A. K., Bianchi, F.,
889 Breitenlechner, M., Brilke, S., Chen, X., Craven, J., Dias, A., Ehrhart, S., Flagan, R. C., Franchin, A., Fuchs, C.,
890 Guida, R., Hakala, J., Hoyle, C. R., Jokinen, T., Junninen, H., Kangasluoma, J., Kim, J., Krapf, M., Kürten, A.,
891 Laaksonen, A., Lehtipalo, K., Makhmutov, V., Mathot, S., Molteni, U., Onnela, A., Peräkylä, O., Piel, F., Petäjä,
892 T., Praplan, A. P., Pringle, K., Rap, A., Richards, N. A., Riipinen, I., Rissanen, M. P., Rondo, L., Sarnela, N.,
893 Schobesberger, S., Scott, C. E., Seinfeld, J. H., Sipilä, M., Steiner, G., Stozhkov, Y., Stratmann, F., Tomé, A.,
894 Virtanen, A., Vogel, A. L., Wagner, A. C., Wagner, P. E., Weingartner, E., Wimmer, D., Winkler, P. M., Ye, P.,
895 Zhang, X., Hansel, A., Dommen, J., Donahue, N. M., Worsnop, D. R., Baltensperger, U., Kulmala, M., Carslaw,
896 K. S., and Curtius, J.: Ion-induced nucleation of pure biogenic particles, *Nature*, 533, 521-526,
897 10.1038/nature17953, 2016.

898 Klinger, L. F., Li, Q. J., Guenther, A. B., Greenberg, J. P., Baker, B., and Bai, J. H.: Assessment of volatile organic
899 compound emissions from ecosystems of China, *J. Geophys. Res.-Atmos.*, 107, 10.1029/2001jd001076, 2002.

900 Kontkanen, J., Paasonen, P., Aalto, J., Bäck, J., Rantala, P., Petäjä, T., and Kulmala, M.: Simple proxies for estimating the
901 concentrations of monoterpenes and their oxidation products at a boreal forest site, *Atmos. Chem. Phys.*, 16,
902 13291-13307, 10.5194/acp-16-13291-2016, 2016.

903 Kulmala, M., Petäjä, T., Nieminen, T., Sipilä, M., Manninen, H. E., Lehtipalo, K., Dal Maso, M., Aalto, P. P., Junninen, H.,
904 Paasonen, P., Riipinen, I., Lehtinen, K. E. J., Laaksonen, A., and Kerminen, V.-M.: Measurement of the nucleation
905 of atmospheric aerosol particles, *Nat. Protoc.*, 7, 1651-1667, 10.1038/nprot.2012.091, 2012.

906 Kurtén, T., Møller, K. H., Nguyen, T. B., Schwantes, R. H., Misztal, P. K., Su, L., Wennberg, P. O., Fry, J. L., and Kjaergaard,
907 H. G.: Alkoxy Radical Bond Scissions Explain the Anomalously Low Secondary Organic Aerosol and
908 Organonitrate Yields From α -Pinene + NO₃, *J. Phys. Chem. Lett.*, 8, 2826-2834, 10.1021/acs.jpcclett.7b01038,
909 2017.

910 Lee, B. H., Mohr, C., Lopez-Hilfiker, F. D., Lutz, A., Hallquist, M., Lee, L., Romer, P., Cohen, R. C., Iyer, S., Kurten, T.,
911 Hu, W., Day, D. A., Campuzano-Jost, P., Jimenez, J. L., Xu, L., Ng, N. L., Guo, H., Weber, R. J., Wild, R. J.,
912 Brown, S. S., Koss, A., de Gouw, J., Olson, K., Goldstein, A. H., Seco, R., Kim, S., McAvey, K., Shepson, P. B.,
913 Starn, T., Baumann, K., Edgerton, E. S., Liu, J., Shilling, J. E., Miller, D. O., Brune, W., Schobesberger, S.,
914 D'Ambro, E. L., and Thornton, J. A.: Highly functionalized organic nitrates in the southeast United States:
915 Contribution to secondary organic aerosol and reactive nitrogen budgets, *P. Natl. Acad. Sci. USA*, 113, 1516-1521,
916 10.1073/pnas.1508108113, 2016.

917 Liu, Y., Nie, W., Li, Y., Ge, D., Liu, C., Xu, Z., Chen, L., Wang, T., Wang, L., Sun, P., Qi, X., Wang, J., Xu, Z., Yuan, J.,
918 Yan, C., Zhang, Y., Huang, D., Wang, Z., Donahue, N. M., Worsnop, D., Chi, X., Ehn, M., and Ding, A.: Formation
919 of condensable organic vapors from anthropogenic and biogenic volatile organic compounds (VOCs) is strongly
920 perturbed by NO_x in eastern China, *Atmos. Chem. Phys.*, 21, 14789-14814, 10.5194/acp-21-14789-2021, 2021.

921 Massoli, P., Stark, H., Canagaratna, M. R., Krechmer, J. E., Xu, L., Ng, N. L., Mauldin, R. L., Yan, C., Kimmel, J., Misztal,
922 P. K., Jimenez, J. L., Jayne, J. T., and Worsnop, D. R.: Ambient Measurements of Highly Oxidized Gas-Phase
923 Molecules during the Southern Oxidant and Aerosol Study (SOAS) 2013, *ACS Earth Space Chem.*, 2, 653-672,
924 10.1021/acsearthspacechem.8b00028, 2018.

925 McDonald, B. C., de Gouw, J. A., Gilman, J. B., Jathar, S. H., Akherati, A., Cappa, C. D., Jimenez, J. L., Lee-Taylor, J.,
926 Hayes, P. L., McKeen, S. A., Cui, Y. Y., Kim, S.-W., Gentner, D. R., Isaacman-VanWertz, G., Goldstein, A. H.,
927 Harley, R. A., Frost, G. J., Roberts, J. M., Ryerson, T. B., and Trainer, M.: Volatile chemical products emerging as
928 largest petrochemical source of urban organic emissions, *Science*, 359, 760-764, 10.1126/science.aaq0524, 2018.

929 McFiggans, G., Mentel, T. F., Wildt, J., Pullinen, I., Kang, S., Kleist, E., Schmitt, S., Springer, M., Tillmann, R., Wu, C.,
930 Zhao, D. F., Hallquist, M., Faxon, C., Le Breton, M., Hallquist, A. M., Simpson, D., Bergström, R., Jenkin, M. E.,
931 Ehn, M., Thornton, J. A., Alfarra, M. R., Bannan, T. J., Percival, C. J., Priestley, M., Topping, D., and Kiendler-
932 Scharr, A.: Secondary organic aerosol reduced by mixture of atmospheric vapours, *Nature*, 565, 587-593,
933 10.1038/s41586-018-0871-y, 2019.

934 Mentel, T. F., Springer, M., Ehn, M., Kleist, E., Pullinen, I., Kurtén, T., Rissanen, M., Wahner, A., and Wildt, J.: Formation
935 of highly oxidized multifunctional compounds: autoxidation of peroxy radicals formed in the ozonolysis of
936 alkenes – deduced from structure–product relationships, *Atmos. Chem. Phys.*, 15, 6745-6765, 10.5194/acp-15-
937 6745-2015, 2015.

938 Mohr, C., Thornton, J. A., Heitto, A., Lopez-Hilfiker, F. D., Lutz, A., Riipinen, I., Hong, J., Donahue, N. M., Hallquist, M.,
939 Petäjä, T., Kulmala, M., and Yli-Juuti, T.: Molecular identification of organic vapors driving atmospheric
940 nanoparticle growth, *Nat. Commun.*, 10, 4442, <https://doi.org/10.1038/s41467-019-12473-2>, 2019.

941 Mutzel, A., Zhang, Y., Böge, O., Rodigast, M., Kolodziejczyk, A., Wang, X., and Herrmann, H.: Importance of secondary
942 organic aerosol formation of α -pinene, limonene, and m-cresol comparing day- and nighttime radical chemistry,
943 *Atmos. Chem. Phys.*, 21, 8479-8498, 10.5194/acp-21-8479-2021, 2021.

944 Nah, T., Sanchez, J., Boyd, C. M., and Ng, N. L.: Photochemical Aging of α -pinene and β -pinene Secondary Organic
945 Aerosol formed from Nitrate Radical Oxidation, *Environ. Sci. Technol.*, 50, 222-231, 10.1021/acs.est.5b04594,
946 2016.

947 Nazaroff, W. W. and Weschler, C. J.: Cleaning products and air fresheners: exposure to primary and secondary air pollutants,
948 *Atmos. Environ.*, 38, 2841-2865, 10.1016/j.atmosenv.2004.02.040, 2004.

949 Ng, N. L., Kwan, A. J., Surratt, J. D., Chan, A. W. H., Chhabra, P. S., Sorooshian, A., Pye, H. O. T., Crouse, J. D., Wennberg,
950 P. O., Flagan, R. C., and Seinfeld, J. H.: Secondary organic aerosol (SOA) formation from reaction of isoprene
951 with nitrate radicals (NO₃), *Atmos. Chem. Phys.*, 8, 4117-4140, 10.5194/acp-8-4117-2008, 2008.

952 Nie, W., Yan, C., Huang, D. D., Wang, Z., Liu, Y., Qiao, X., Guo, Y., Tian, L., Zheng, P., Xu, Z., Li, Y., Xu, Z., Qi, X., Sun,
953 P., Wang, J., Zheng, F., Li, X., Yin, R., Dallenbach, K. R., Bianchi, F., Petäjä, T., Zhang, Y., Wang, M., Schervish,
954 M., Wang, S., Qiao, L., Wang, Q., Zhou, M., Wang, H., Yu, C., Yao, D., Guo, H., Ye, P., Lee, S., Li, Y. J., Liu, Y.,
955 Chi, X., Kerminen, V.-M., Ehn, M., Donahue, N. M., Wang, T., Huang, C., Kulmala, M., Worsnop, D., Jiang, J.,
956 and Ding, A.: Secondary organic aerosol formed by condensing anthropogenic vapours over China's megacities,
957 *Nat. Geosci.*, 15, 255-261, 10.1038/s41561-022-00922-5, 2022.

958 Nieminen, T., Lehtinen, K. E. J., and Kulmala, M.: Sub-10 nm particle growth by vapor condensation – effects of vapor
959 molecule size and particle thermal speed, *Atmos. Chem. Phys.*, 10, 9773-9779, 10.5194/acp-10-9773-2010, 2010.

960 Novelli, A., Cho, C., Fuchs, H., Hofzumahaus, A., Rohrer, F., Tillmann, R., Kiendler-Scharr, A., Wahner, A., and Vereecken,

961 L.: Experimental and theoretical study on the impact of a nitrate group on the chemistry of alkoxy radicals, *Phys.*
962 *Chem. Chem. Phys.*, 23, 5474-5495, 10.1039/d0cp05555g, 2021.

963 Ortega, I. K., Suni, T., Boy, M., Grönholm, T., Manninen, H. E., Nieminen, T., Ehn, M., Junninen, H., Hakola, H., Hellén,
964 H., Valmari, T., Arvela, H., Zegelin, S., Hughes, D., Kitchen, M., Cleugh, H., Worsnop, D. R., Kulmala, M., and
965 Kerminen, V. M.: New insights into nocturnal nucleation, *Atmos. Chem. Phys.*, 12, 4297-4312, 10.5194/acp-12-
966 4297-2012, 2012.

967 Pagonis, D., Algrim, L. B., Price, D. J., Day, D. A., Handschy, A. V., Stark, H., Miller, S. L., de Gouw, J. A., Jimenez, J. L.,
968 and Ziemann, P. J.: Autoxidation of Limonene Emitted in a University Art Museum, *Environ. Sci. Tech. Let.*, 6,
969 520-524, 10.1021/acs.estlett.9b00425, 2019.

970 Peng, C., Wang, W., Li, K., Li, J., Zhou, L., Wang, L., and Ge, M.: The Optical Properties of Limonene Secondary Organic
971 Aerosols: The Role of NO₃, OH, and O₃ in the Oxidation Processes, *J. Geophys. Res.-Atmos.*, 123, 3292-3303,
972 <https://doi.org/10.1002/2017JD028090>, 2018.

973 Peräkylä, O., Riva, M., Heikkinen, L., Quéléver, L., Roldin, P., and Ehn, M.: Experimental investigation into the volatilities
974 of highly oxygenated organic molecules (HOMs), *Atmos. Chem. Phys.*, 20, 649-669, 10.5194/acp-20-649-2020,
975 2020.

976 Pullinen, I., Schmitt, S., Kang, S., Sarrafzadeh, M., Schlag, P., Andres, S., Kleist, E., Mentel, T. F., Rohrer, F., Springer, M.,
977 Tillmann, R., Wildt, J., Wu, C., Zhao, D., Wahner, A., and Kiendler-Scharr, A.: Impact of NO_x on secondary
978 organic aerosol (SOA) formation from α-pinene and β-pinene photooxidation: the role of highly oxygenated
979 organic nitrates, *Atmos. Chem. Phys.*, 20, 10125-10147, 10.5194/acp-20-10125-2020, 2020.

980 Pye, H. O. T., Chan, A. W. H., Barkley, M. P., and Seinfeld, J. H.: Global modeling of organic aerosol: the importance of
981 reactive nitrogen (NO_x and NO₃), *Atmos. Chem. Phys.*, 10, 11261-11276, 10.5194/acp-10-11261-2010, 2010.

982 Rissanen, M. P., Kurtén, T., Sipilä, M., Thornton, J. A., Kangasluoma, J., Sarnela, N., Junninen, H., Jørgensen, S., Schallhart,
983 S., Kajos, M. K., Taipale, R., Springer, M., Mentel, T. F., Ruuskanen, T., Petäjä, T., Worsnop, D. R., Kjaergaard,
984 H. G., and Ehn, M.: The formation of highly oxidized multifunctional products in the ozonolysis of cyclohexene,
985 *J. Am. Chem. Soc.*, 136, 15596-15606, 10.1021/ja507146s, 2014.

986 Riva, M., Rantala, P., Krechmer, J. E., Peräkylä, O., Zhang, Y., Heikkinen, L., Garmash, O., Yan, C., Kulmala, M., Worsnop,
987 D., and Ehn, M.: Evaluating the performance of five different chemical ionization techniques for detecting gaseous
988 oxygenated organic species, *Atmos. Meas. Tech.*, 12, 2403-2421, 10.5194/amt-12-2403-2019, 2019.

989 Rohrer, F., Bohn, B., Brauers, T., Brüning, D., Johnen, F. J., Wahner, A., and Kleffmann, J.: Characterisation of the
990 photolytic HONO-source in the atmosphere simulation chamber SAPHIR, *Atmos. Chem. Phys.*, 5, 2189-2201,
991 10.5194/acp-5-2189-2005, 2005.

992 Rollins, A. W., Browne, E. C., Min, K.-E., Pusede, S. E., Wooldridge, P. J., Gentner, D. R., Goldstein, A. H., Liu, S., Day,
993 D. A., Russell, L. M., and Cohen, R. C.: Evidence for NO_x control over nighttime SOA formation, *Science*, 337,
994 1210-1212, 10.1126/science.1221520, 2012.

995 Rollins, A. W., Kiendler-Scharr, A., Fry, J. L., Brauers, T., Brown, S. S., Dorn, H. P., Dubé, W. P., Fuchs, H., Mensah, A.,
996 Mentel, T. F., Rohrer, F., Tillmann, R., Wegener, R., Wooldridge, P. J., and Cohen, R. C.: Isoprene oxidation by
997 nitrate radical: alkyl nitrate and secondary organic aerosol yields, *Atmos. Chem. Phys.*, 9, 6685-6703,
998 10.5194/acp-9-6685-2009, 2009.

999 Saunders, S. M., Jenkin, M. E., Derwent, R. G., and Pilling, M. J.: Protocol for the development of the Master Chemical
1000 Mechanism, MCM v3 (Part A): tropospheric degradation of non-aromatic volatile organic compounds, *Atmos.*
1001 *Chem. Phys.*, 3, 161-180, 2003a.

1002 Saunders, S. M., Jenkin, M. E., Derwent, R. G., and Pilling, M. J.: Protocol for the development of the Master Chemical
1003 Mechanism, MCM v3 (Part A): tropospheric degradation of non-aromatic volatile organic compounds, *Atmos.*
1004 *Chem. Phys.*, 3, 161-180, 10.5194/acp-3-161-2003, 2003b.

1005 Schervish, M. and Donahue, N. M.: Peroxy radical chemistry and the volatility basis set, *Atmos. Chem. Phys.*, 20, 1183-
1006 1199, 10.5194/acp-20-1183-2020, 2020.

1007 Seinfeld, J. H. and Pandis, S. N.: *Atmospheric Chemistry and Physics: From Air Pollution to Climate Change*, 2nd ed,
1008 Wiley, John & Sons, New York, 2006.

1009 Shen, H., Zhao, D., Pullinen, I., Kang, S., Vereecken, L., Fuchs, H., Acir, I.-H., Tillmann, R., Rohrer, F., Wildt, J., Kiendler-
1010 Scharr, A., Wahner, A., and Mentel, T. F.: Highly Oxygenated Organic Nitrates Formed from NO₃ Radical-Initiated
1011 Oxidation of β -Pinene, *Environ. Sci. Technol.*, 10.1021/acs.est.1c03978, 2021.

1012 Shrivastava, M., Cappa, C. D., Fan, J., Goldstein, A. H., Guenther, A. B., Jimenez, J. L., Kuang, C., Laskin, A., Martin, S.
1013 T., Ng, N. L., Petäjä, T., Pierce, J. R., Rasch, P. J., Roldin, P., Seinfeld, J. H., Shilling, J., Smith, J. N., Thornton,
1014 J. A., Volkamer, R., Wang, J., Worsnop, D. R., Zaveri, R. A., Zelenyuk, A., and Zhang, Q.: Recent advances in
1015 understanding secondary organic aerosol: Implications for global climate forcing, *Rev. Geophys.*, 55, 509-559,
1016 10.1002/2016rg000540, 2017.

1017 Slade, J. H., de Perre, C., Lee, L., and Shepson, P. B.: Nitrate radical oxidation of γ -terpinene: hydroxy nitrate, total
1018 organic nitrate, and secondary organic aerosol yields, *Atmos. Chem. Phys.*, 17, 8635-8650, 10.5194/acp-17-8635-
1019 2017, 2017.

1020 Spittler, M., Barnes, I., Bejan, I., Brockmann, K. J., Benter, T., and Wirtz, K.: Reactions of NO₃ radicals with limonene and
1021 α -pinene: Product and SOA formation, *Atmos. Environ.*, 40, 116-127, 10.1016/j.atmosenv.2005.09.093, 2006.

1022 Takeuchi, M. and Ng, N. L.: Chemical composition and hydrolysis of organic nitrate aerosol formed from hydroxyl and
1023 nitrate radical oxidation of α -pinene and β -pinene, *Atmos. Chem. Phys.*, 19, 12749-12766, 10.5194/acp-19-12749-
1024 2019, 2019.

1025 Tröstl, J., Chuang, W. K., Gordon, H., Heinritzi, M., Yan, C., Molteni, U., Ahlm, L., Frege, C., Bianchi, F., Wagner, R.,
1026 Simon, M., Lehtipalo, K., Williamson, C., Craven, J. S., Duplissy, J., Adamov, A., Almeida, J., Bernhammer, A.
1027 K., Breitenlechner, M., Brilke, S., Dias, A., Ehrhart, S., Flagan, R. C., Franchin, A., Fuchs, C., Guida, R., Gysel,
1028 M., Hansel, A., Hoyle, C. R., Jokinen, T., Junninen, H., Kangasluoma, J., Keskinen, H., Kim, J., Krapf, M., Kürten,
1029 A., Laaksonen, A., Lawler, M., Leiminger, M., Mathot, S., Möhler, O., Nieminen, T., Onnela, A., Petäjä, T., Piel,
1030 F. M., Miettinen, P., Rissanen, M. P., Rondo, L., Sarnela, N., Schobesberger, S., Sengupta, K., Sipilä, M., Smith,
1031 J. N., Steiner, G., Tomè, A., Virtanen, A., Wagner, A. C., Weingartner, E., Wimmer, D., Winkler, P. M., Ye, P.,
1032 Carslaw, K. S., Curtius, J., Dommen, J., Kirkby, J., Kulmala, M., Riipinen, I., Worsnop, D. R., Donahue, N. M.,
1033 and Baltensperger, U.: The role of low-volatility organic compounds in initial particle growth in the atmosphere,
1034 *Nature*, 533, 527-531, 10.1038/nature18271, 2016.

1035 Vereecken, L. and Nozière, B.: H migration in peroxy radicals under atmospheric conditions, *Atmos. Chem. Phys.*, 20,
1036 7429-7458, 10.5194/acp-20-7429-2020, 2020.

1037 Vereecken, L. and Peeters, J.: Decomposition of substituted alkoxy radicals-part I: a generalized structure-activity
1038 relationship for reaction barrier heights, *Phys. Chem. Chem. Phys.*, 11, 9062-9074, 10.1039/b909712k, 2009.

1039 Vereecken, L. and Peeters, J.: A structure-activity relationship for the rate coefficient of H-migration in substituted alkoxy
1040 radicals, *Phys. Chem. Chem. Phys.*, 12, 12608-12620, 10.1039/c0cp00387e, 2010.

1041 Wagner, N. L., Dubé, W. P., Washenfelder, R. A., Young, C. J., Pollack, I. B., Ryerson, T. B., and Brown, S. S.: Diode laser-
1042 based cavity ring-down instrument for NO₃, N₂O₅, NO, NO₂ and O₃ from aircraft, *Atmos. Meas. Tech.*, 4, 1227-
1043 1240, 10.5194/amt-4-1227-2011, 2011.

1044 Wang, H., Ma, X., Tan, Z., Wang, H., Chen, X., Chen, S., Gao, Y., Liu, Y., Liu, Y., Yang, X., Yuan, B., Zeng, L., Huang, C.,
1045 Lu, K., and and Zhang, Y.: Anthropogenic monoterpenes aggravating ozone pollution, *Natl. Sci. Rev.*, nwac103,
1046 10.1093/nsr/nwac103, 2022.

1047 Wang, S. and Pratt, K. A.: Molecular Halogens Above the Arctic Snowpack: Emissions, Diurnal Variations, and Recycling
1048 Mechanisms, *J. Geophys. Res.-Atmos.*, 122, 11991-12007, 10.1002/2017jd027175, 2017.

1049 Wu, C., Bell, D. M., Graham, E. L., Haslett, S., Riipinen, I., Baltensperger, U., Bertrand, A., Giannoukos, S., Schoonbaert,
1050 J., El Haddad, I., Prevot, A. S. H., Huang, W., and Mohr, C.: Photolytically induced changes in composition and
1051 volatility of biogenic secondary organic aerosol from nitrate radical oxidation during night-to-day transition,
1052 *Atmos. Chem. Phys.*, 21, 14907-14925, 10.5194/acp-21-14907-2021, 2021a.

1053 Wu, R., Vereecken, L., Tsiligiannis, E., Kang, S., Albrecht, S. R., Hantschke, L., Zhao, D., Novelli, A., Fuchs, H., Tillmann,
1054 R., Hohaus, T., Carlsson, P. T. M., Shenolikar, J., Bernard, F., Crowley, J. N., Fry, J. L., Brownwood, B., Thornton,
1055 J. A., Brown, S. S., Kiendler-Scharr, A., Wahner, A., Hallquist, M., and Mentel, T. F.: Molecular composition and
1056 volatility of multi-generation products formed from isoprene oxidation by nitrate radical, *Atmos. Chem. Phys.*,
1057 21, 10799-10824, 10.5194/acp-21-10799-2021, 2021b.

1058 Xu, L., Guo, H., Boyd, C. M., Klein, M., Bougiatioti, A., Cerully, K. M., Hite, J. R., Isaacman-VanWertz, G., Kreisberg,
1059 N. M., Knote, C., Olson, K., Koss, A., Goldstein, A. H., Hering, S. V., de Gouw, J., Baumann, K., Lee, S.-H.,
1060 Nenes, A., Weber, R. J., and Ng, N. L.: Effects of anthropogenic emissions on aerosol formation from isoprene
1061 and monoterpenes in the southeastern United States, *P. Natl. Acad. Sci. USA*, 112, 37-42,
1062 10.1073/pnas.1417609112, 2015.

1063 Yan, C., Nie, W., Äijälä, M., Rissanen, M. P., Canagaratna, M. R., Massoli, P., Junninen, H., Jokinen, T., Sarnela, N., Häme,
1064 S. A. K., Schobesberger, S., Canonaco, F., Yao, L., Prévôt, A. S. H., Petäjä, T., Kulmala, M., Sipilä, M., Worsnop,
1065 D. R., and Ehn, M.: Source characterization of highly oxidized multifunctional compounds in a boreal forest
1066 environment using positive matrix factorization, *Atmos. Chem. Phys.*, 16, 12715-12731, 10.5194/acp-16-12715-
1067 2016, 2016.

1068 Zhang, H., Yee, L. D., Lee, B. H., Curtis, M. P., Worton, D. R., Isaacman-VanWertz, G., Offenberg, J. H., Lewandowski,
1069 M., Kleindienst, T. E., Beaver, M. R., Holder, A. L., Lonneman, W. A., Docherty, K. S., Jaoui, M., Pye, H. O. T.,
1070 Hu, W., Day, D. A., Campuzano-Jost, P., Jimenez, J. L., Guo, H., Weber, R. J., de Gouw, J., Koss, A. R., Edgerton,
1071 E. S., Brune, W., Mohr, C., Lopez-Hilfiker, F. D., Lutz, A., Kreisberg, N. M., Spielman, S. R., Hering, S. V.,
1072 Wilson, K. R., Thornton, J. A., and Goldstein, A. H.: Monoterpenes are the largest source of summertime organic
1073 aerosol in the southeastern United States, *P. Natl. Acad. Sci. USA*, 115, 2038-2043, 10.1073/pnas.1717513115,
1074 2018.

1075 Zhao, D., Pullinen, I., Fuchs, H., Schrade, S., Wu, R., Acir, I.-H., Tillmann, R., Rohrer, F., Wildt, J., Guo, Y., Kiendler-
1076 Scharr, A., Wahner, A., Kang, S., Vereecken, L., and Mentel, T. F.: Highly oxygenated organic molecule (HOM)
1077 formation in the isoprene oxidation by NO₃ radical, *Atmos. Chem. Phys.*, 21, 9681-9704, 10.5194/acp-21-9681-
1078 2021, 2021.

1079 Zhao, D., Schmitt, S. H., Wang, M., Acir, I.-H., Tillmann, R., Tan, Z., Novelli, A., Fuchs, H., Pullinen, I., Wegener, R.,
1080 Rohrer, F., Wildt, J., Kiendler-Scharr, A., Wahner, A., and Mentel, T. F.: Effects of NO_x and SO₂ on the secondary
1081 organic aerosol formation from photooxidation of α -pinene and limonene, *Atmos. Chem. Phys.*, 18, 1611-1628,
1082 10.5194/acp-18-1611-2018, 2018.

1083 Zhao, D. F., Buchholz, A., Kortner, B., Schlag, P., Rubach, F., Kiendler-Scharr, A., Tillmann, R., Wahner, A., Flores, J. M.,
1084 Rudich, Y., Watne, Å. K., Hallquist, M., Wildt, J., and Mentel, T. F.: Size-dependent hygroscopicity parameter (κ)
1085 and chemical composition of secondary organic cloud condensation nuclei, *Geophys. Res. Lett.*, 42, 10920-10928,
1086 10.1002/2015gl066497, 2015a.

1087 Zhao, D. F., Kaminski, M., Schlag, P., Fuchs, H., Acir, I. H., Bohn, B., Häseler, R., Kiendler-Scharr, A., Rohrer, F., Tillmann,
1088 R., Wang, M. J., Wegener, R., Wildt, J., Wahner, A., and Mentel, T. F.: Secondary organic aerosol formation from
1089 hydroxyl radical oxidation and ozonolysis of monoterpenes, *Atmos. Chem. Phys.*, 15, 991-1012, 10.5194/acp-15-
1090 991-2015, 2015b.

1091 Zhou, L., Gierens, R., Sogachev, A., Mogensen, D., Ortega, J., Smith, J. N., Harley, P. C., Prenni, A. J., Levin, E. J. T.,
1092 Turnipseed, A., Rusanen, A., Smolander, S., Guenther, A. B., Kulmala, M., Karl, T., and Boy, M.: Contribution

1093 from biogenic organic compounds to particle growth during the 2010 BEACHON-ROCS campaign in a Colorado
1094 temperate needleleaf forest, *Atmos. Chem. Phys.*, 15, 8643-8656, 10.5194/acp-15-8643-2015, 2015.
1095 Ziemann, P. J. and Atkinson, R.: Kinetics, products, and mechanisms of secondary organic aerosol formation, *Chem. Soc.*
1096 *Rev.*, 41, 6582-6605, 10.1039/c2cs35122f, 2012.
1097